

Article

Evaluation of Cherts in Gumushane Province in Terms of Alkali Silica Reaction

Demet Demir Şahin 

Mining Technology Program, Department of Mining and Mineral Extraction, Gumushane University, 29000 Gumushane, Turkey; demetsahin@gumushane.edu.tr or demetdemir2929@hotmail.com

Abstract: Alkali–silica reaction (ASR) occurs when alkali oxides coming from the cement composition in concrete come together with reactive silica and moisture coming from the aggregate. Additional maintenance and repair costs caused by the development of ASR in concrete cause the cost to increase. However, thanks to the measures taken against ASR in the early period, it contributes to the creation of sustainable and durable concrete structures. The article investigated the usability of cherts with eight different chemical compositions as aggregates in ready-mixed concrete plants in Gümüşhane. Cherts have been investigated for alkaline reactivity and are intended to be used largely as a source for concrete plants. ASR length changes of the samples prepared according to ASTM C1260 standard were determined after 3, 7, 14, and 28 days of the curing period. Microstructural examination, ultrasonic P-wave velocity, and bending and compressive strength experiments supporting ASR were carried out. The obtained test results were compared between the reference (limestone) sample and each other, as well as with the values specified in the standards. The compressive and bending strength values of the samples increase depending on their ASR. It was observed that the crack structures and types increased depending on the increase in the crack values.

Keywords: ASR; concrete; chert; reactive aggregate; limestone; expansion



Citation: Demir Şahin, D. Evaluation of Cherts in Gumushane Province in Terms of Alkali Silica Reaction. *Buildings* **2024**, *14*, 873. <https://doi.org/10.3390/buildings14040873>

Academic Editor: Mohamed K. Ismail

Received: 8 February 2024

Revised: 5 March 2024

Accepted: 19 March 2024

Published: 23 March 2024

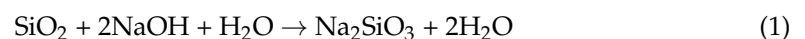


Copyright: © 2024 by the author. Licensee MDPI, Basel, Switzerland. This article is an open access article distributed under the terms and conditions of the Creative Commons Attribution (CC BY) license (<https://creativecommons.org/licenses/by/4.0/>).

1. Introduction

Concrete, a globally fundamental construction material, represents a significant investment for national economies. Approximately 60–75% of this material consists of aggregate components, with around 10–15% comprising Portland cement or cementitious materials, along with water [1–3]. In the current era characterized by advanced technologies and finite natural resources, the production of concrete is expected to yield long life, contribute to environmental and public health, exhibit resilience to external influences, require minimal maintenance, and entail low costs [4]. Attention must be paid to the selection of aggregates, a crucial component of concrete. The chemical composition of aggregates, which are rich in compounds such as reactive SiO₂, holds significance in generating detrimental reactions within concrete. Particularly, aggregates with high silica content, strong alkali components, water, and high humidity significantly contribute to the initiation of alkali–silica reaction (ASR), a crucial factor in the deterioration of concrete [5–8].

These reactions result in substantial damage to both concrete and mortar, causing significant structural impairment [9–11]. The resolution of this damage is intricate and often demands substantial financial resources [12–15]. ASR manifests as a chemical reaction between the reactive silica in aggregates and the hydroxyl ions in the concrete pore solution (Equation (1)).

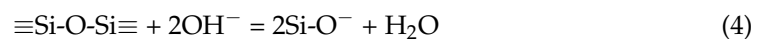
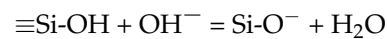


The alkali–silica reaction (ASR) converts the siloxane (Si–O–Si) bonds in the aggregate composition to silanol (Si–OH) bonds, primarily influenced by the elevated pH in the pore solution. Aggregates with a high water content in their porous structure,

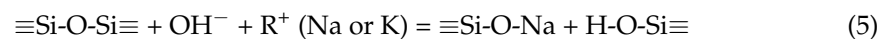
especially those containing opal, exhibit an abundance of silanol bonds. These bonds possess an acidic nature and react with the alkaline forms present in the pore solution. Silanol groups, upon a second attack by hydroxyl ions, transform into the SiO-form and disperse in water. Positively charged ions, such as sodium, potassium, and calcium, attract and encapsulate the negatively charged SiO-gel, leading to the formation of Equation (2) [16,17].



Following the reaction, the siloxane bridge undergoes damage under the influence of hydroxyl ions, transforming into the SiO-form, resulting in swelling and the formation of a water-absorbing gel. Subsequently, the damaged area and its surroundings initiate the development of fine hairline cracks [18]. Chemical passivity characterizes the (SiO₂) in aggregates, particularly in quartz form, which are structurally arranged as (≡Si-O-Si≡). However, the irregularities on the surface of crystalline silica, their water-absorbing capability, and amorphous structure [≡Si-OH]) enhance their tendency to dissolve [19]. Consequently, silica particles exhibit a high susceptibility to dissolution. They first react with hydroxyl ions through (≡Si-OH) and, subsequently, through the neutralization of (≡Si-O-Si≡), as depicted in Equations (3) and (4).



Sodium hydroxide (NaOH) and potassium hydroxide (KOH) from the pore solution of concrete, calcium hydroxide (Ca(OH)₂) produced during cement hydration, and alkali-silicate solution and gel (depending on humidity levels) begin to react. The reaction between ≡Si-O-Si≡ and hydroxyl ions intensifies further (Equations (5)–(7)) [20].



Following the aforementioned reactions, the alkali-silica gel penetrates the cement paste within the aggregates in concrete, initiating a reaction with it. The presence of moisture in the environment leads to expansion, stresses on the interface of the cement paste, expansion, and the formation of cracks. Reactive amorphous and weak crystal structures in natural aggregates and hydroxyl ions, along with factors such as Portland cement, aggregate particle size, admixtures, and the concrete pore solution, induce chemical reactions affecting the durability of concrete.

Concrete, being an integral element of structures, signifies strength and durability when it exhibits high-quality properties. Changes in such properties of concrete result from interactions between aggregates and cement paste, causing detrimental effects on concrete [21]. Alkali-silica reaction (ASR) is a significant phenomenon. This reaction, through a series of alterations in concrete, reduces the strength of the cement paste, leading to expansion and crack formation in concrete, thereby diminishing its strength and resistance to freezing [19,22,23]. Factors triggering alkali-silica reaction (ASR) include the type of aggregate and binder, the amorphous or crystalline state of reactive aggregates, the quantity and distribution of reactive aggregates, environmental conditions surrounding the aggregates, and various external stimulating factors, all contributing to destructive and lasting damages in concrete [24,25].

As alkali-silica reaction (ASR) induces expansion in concrete, it leads to structural damage [26,27].

The reactivity of the silica component in the composition of aggregates depends on the mineral structure. The silica component can exhibit different textures and compositions in each rock. This is primarily due to the cooling rate during the formation of rocks, which can result in either an amorphous or crystalline structure. The solubility of the silica component is higher in alkaline or acidic environments, while its solubility is lower in a neutral pH condition [28,29]. The reactivity of silica-containing aggregates is determined by the free energy of quartz. The free energy determines the solubility of quartz based on defects in the cage structure and the degree of crystallization [30]. Studies on the amorphous and crystalline structure of quartz have determined which structure is more reactive. Crystalline quartz is less soluble than amorphous quartz in a corrosive environment with a high pH ratio. This is because the amorphous structure of the aggregate, with its cracks and irregularities, allows the ions formed by ASR to penetrate the aggregate more easily than in the crystalline structure. The quality and geological characteristics of silica within crystalline quartz, such as strained quartz during formation, can contribute to its reactive nature [31]. Minerals formed rapidly due to quick cooling, such as cristobalite and tridymite, may exhibit reactive properties at normal temperatures [27,32]. Additionally, certain rocks with reactive silica include chert, some volcanic glasses, certain clays, phyllites, metamorphic breccias, as well as breccias, phyllites, schists, gneisses, gneiss granite, vein quartz, quartzite, and high-metamorphic rocks containing sandstone. However, it is not possible to definitively state that containing reactive silica will lead to ASR formation because factors such as fine-grained silica increasing contact surface with alkalis contribute to increased reactivity [18,33].

The degree of porosity of aggregate particles also plays a crucial role in the rate of ASR expansion. A higher degree of porosity allows moisture to easily penetrate into the aggregate and concrete and facilitates the easy dispersion of alkali ions [27,34].

The particle size of aggregates has an impact on reactivity. Fine-grained aggregates have silica minerals with less structural order and are more prone to instability compared to coarse-grained aggregates [32]. Particularly, when the particle size is below the given limit (~0.02–0.07 mm), it leads to less expansion, reducing the rate and amount of expansion. Coarse-grained aggregates exhibit a high expansion rate in prolonged expansion, while fine-grained reactive aggregates have a higher reaction rate [35–38]. Researchers have varying views on the influence of aggregate particle size on ASR formation. Some suggest that a fine aggregate size has a mitigating effect on ASR [23,39]. Coarse aggregates are more sensitive to ASR compared to fine aggregates. This is because fine-grained aggregates participate in pozzolanic reactions early on, converting alkali-silica gel into calcium silicate hydrate, reducing the alkali level in the solution, and promoting pozzolanic reaction [40]. The use of aggregates with particle sizes between 1 and 5 mm ensures maximum expansion [41]. It has been observed that coarse-grained aggregates cause less expansion compared to fine-grained aggregates, and reactive fine aggregates result in slow and prolonged expansion [42]. Fine reactive aggregates initiate expansion in the early stages and maintain it, while coarse reactive aggregates cause slow and prolonged expansion. As the particle size of silica-containing aggregate decreases below 0.15–10 mm, the ASR expansion increases, the cement/aggregate ratio for maximum expansion decreases, and the expansion progresses slowly [43].

The morphological structure of aggregates also influences ASR. Aggregates become angular when crushed and reduced in size. Studies have explored the impact of particle shape on ASR. Aggregates with the same type of reactive round particle structure exhibit different ASR development characteristics compared to aggregates prepared by crushing for the ASTM C1260 accelerated mortar bar test [10]. The expansion characteristics obtained by using natural and crushed aggregates of medium size at a 25% ratio differ. It has been found that reactive particle size is more effective in crushed aggregates, small and large angular particles are not effective, but medium-sized angular particles influence expansion [44].

It has been emphasized in various studies that the chemical composition alone of aggregates is not sufficient as a factor for alkali-silica reaction (ASR) formation. The reactive silica and alkali content of aggregates, particle size, particle structure, and porosity status can alter the impact value. Aggregates with amorphous, glassy, microporous structures, and a large surface area, along with numerous cage defects, have a higher potential for initiating reactions (Farny and Kosmatka, 1997) [32]. Specifically, the fine-grained nature of aggregates, a large surface area, and a dense structure of cracks and pores contribute to increased reactivity [45].

- -Alkali + Reactive Silica → Alkaline Silica Gel Products
- -Alkaline Silica Gel Products + Humidity → Expansion

The presence of alkali-silica reaction (ASR) gel does not directly cause deterioration in concrete. However, high moisture or humidity in the surrounding environment leads to expansion and an increase in internal pressure. If the resulting stresses gradually exceed the tensile stresses, it can lead to the formation of cracks and, ultimately, deterioration. The ASR formation mechanism occurs as described below (Figure 1) [29,46–49].

The gel formed after the reaction does not necessarily cause significant damage to concrete every time. For the gel to cause damage, the relative humidity must be 80% or higher, leading to the spread of alkali ions, the formation of gel in reaction zones, swelling due to the absorption of water by the formed gel, and an increase in internal stresses. However, if there is an appropriate level of humidity in the concrete throughout its service life, ASR may not pose a serious threat. To prevent ASR in concrete, strategies such as low water-to-cement ratio, additional cement, mineral additives, or reducing permeability through different methods can be employed. This would hinder the spread of alkalis to the reaction zones by limiting access [50]. Additionally, the design of concrete with reactive silica-containing aggregates should ensure their incorporation into the concrete composition in an appropriate manner. This not only makes more effective use of existing resources but also significantly reduces the need for raw material exploration [51].

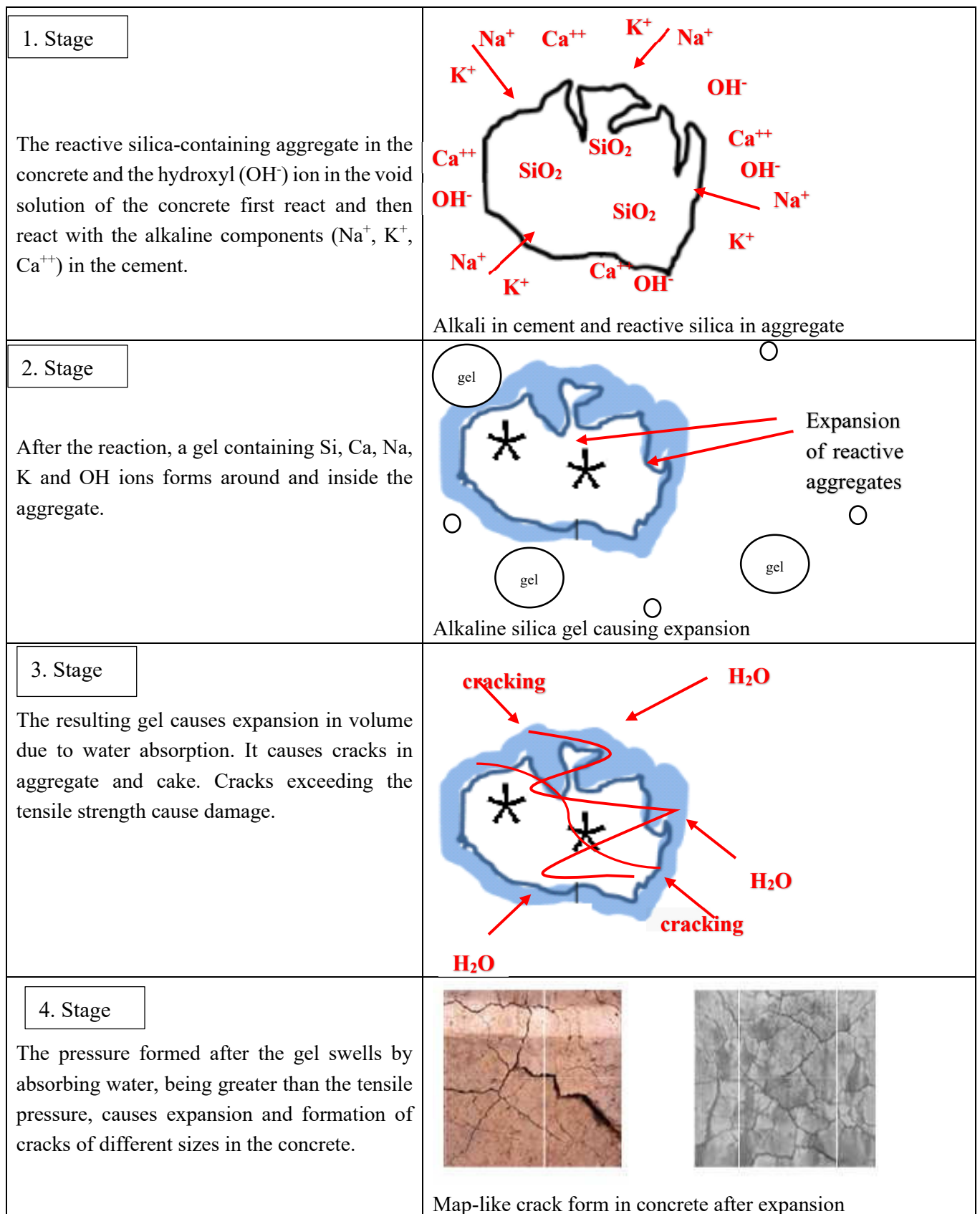


Figure 1. ASR formation mechanisms and phases of reactive aggregate in concrete composition [40,52–56].

Cherts are sedimentary rocks with a cryptocrystalline and microcrystalline structure that can lead to an alkali–silica reaction (ASR) when appropriate conditions are present in concrete. Cherts, when used as aggregates in concrete, act as known activators, causing ASR. This gel absorbs water and generates expansive forces that can lead to cracking, thus hindering the hardening process. However, due to variations in chert composition, it can exhibit different characteristic features regarding its potential to induce reactions [57]. The dissolved silica, silica content, mineralogy, chemical factors, thermodynamic properties, specific surface area, particle size, voids, cracks within particles, and crystallinity in chert composition determine its reactivity, indicating its suitability for use in concrete [58]. If chert has a weak crystalline silica structure, it tends to react with hydroxyl ions, leading to aggregate dissolution. This situation can result in the formation of alkali–silica gel, causing expansion and various durability issues in concrete [59]. The presence of a fine crystal structure in chert increases the reaction surface and enhances its reactivity [60]. Different researchers hold different views on the reactivity of cherts. Nishiyama et al. [61] stated in their study that reactive cherts have low crystallization indices. Jones (1989) [62] argued in his study that the mineralogy of cherts has a more significant impact on their reactivity than other factors.

Chert is found in limestone layers on the earth's surface or as gravel in riverbeds. This natural occurrence indicates its suitability for use as concrete aggregate. Therefore, reactive aggregates like cherts and opals do not exhibit an increasing expansion tendency. If expansion occurs, it reaches a maximum value and then decreases. The point of maximum expansion for reactive aggregates is referred to as “pessimum”, and for cherts, this value is less than 10% and greater than 60% [57]. According to ASTM C33, the required chert content for ASR to occur is accepted as 3% and 8% for fine and coarse aggregates, respectively [63]. McNally and [60] considered 1% chert content as a high-expansion value in accelerated mortar bar tests. However, Gogte (1973) [64] mentioned that 1% chert content is considered high expansion, but it does not pose a problem for use unless the alkali content is high. Swamy (1992) [25] suggested in his study that concrete with more than 5% nonreactive aggregate or more than 60% chert is considered to have a low probability of being reactive.

In this study, chert samples with eight different chemical compositions were collected from various regions within the borders of Gumushane province, and for the comparison of results, limestone aggregate, which is accepted as a reference, was used. The cherts that are widespread in the region were evaluated for their potential to be an alternative concrete aggregate if used in concrete plants, which was determined using the alkali–silica reaction (ASR) elongation values. In this study, the ASTM C1260 Standard Test Method for Potential Alkali Reactivity of Aggregates (mortar-bar method) was employed to determine the alkali–silica reactivity of eight aggregates from different origins [10,29]. Sometimes, even if the aggregate is not reactive, different components may become reactive in a high alkali environment, leading to the occurrence of ASR [65].

This study aimed to identify and take preventive measures against alkali–silica reaction before it occurs in concrete, eliminating later high costs and unavoidable damages. The aggregates used in this study consisted of chert samples obtained from different routes, abundant in the Gumushane region, each having distinct chemical, mineralogical, and morphological structures. Eight chert samples were evaluated for ASR. Concrete samples, conforming to ASTM C 1260 standards, were prepared, and ASR development levels were determined after curing periods of 3, 7, 14, and 28 days. These values were then compared with the reference prepared with only limestone and the limit values specified in the standard. Additionally, chemical reactivity, particle size, water usage, pore structure of the aggregate, specific surface area determination, and concrete's compressive, tensile, and ultrasonic pulse velocity tests were conducted. The results were compared based on numerous parametric data and supported by studies available in the literature.

2. Materials and Methods

The study employed CEM I 42.5 R cement, nonreactive limestone for reference sample production, and chert samples with different chemical compositions from the Gumushane region, named TD, T, AK, GD, AC, GC, BC, and TK, as well as tap water. The origin locations of the aggregates used are provided in Figure 2 and field image Figure 3.

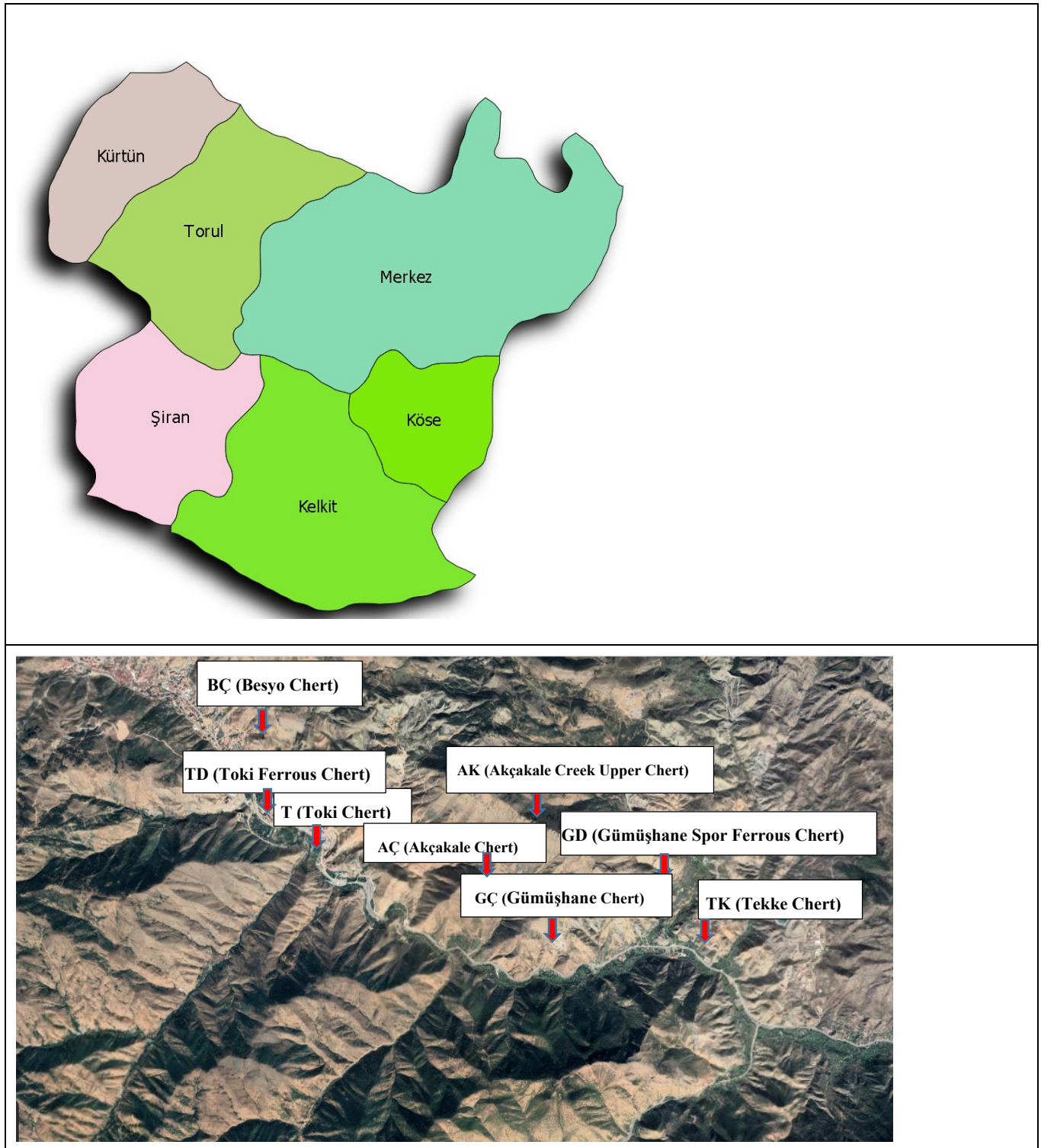


Figure 2. Where the chert is supplied.

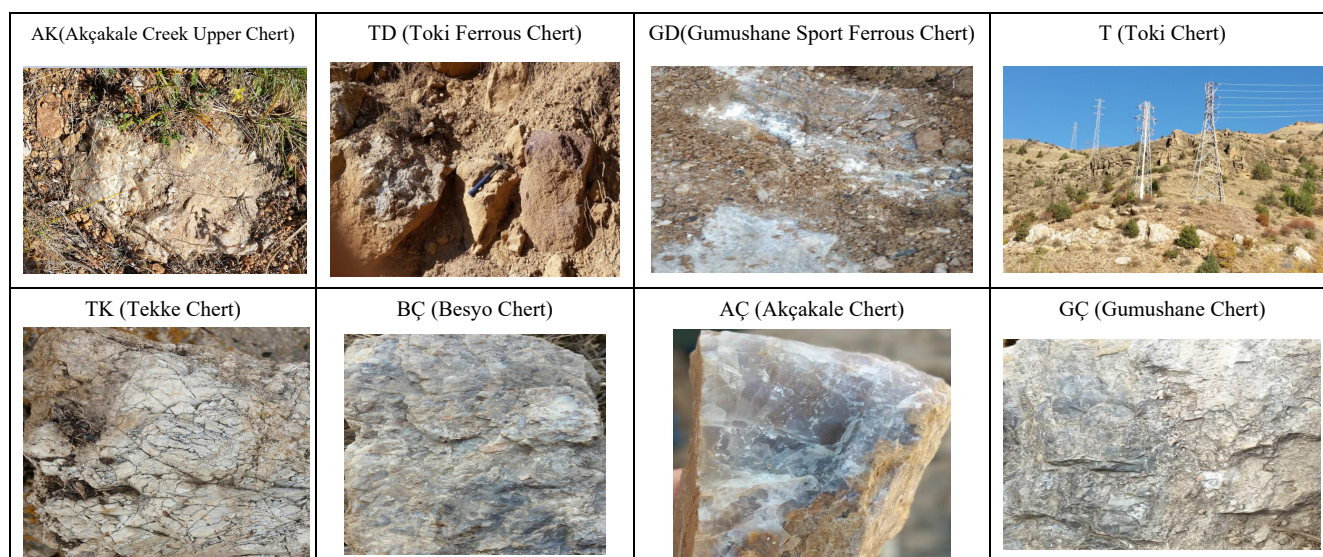


Figure 3. Microscopic field images taken from areas where chert was collected.

2.1. Materials Used in Mortar Mix

The cement used in the mortar mixtures prepared for ASR was sourced from the Askale Cement Factory, which operates within the borders of Gumushane Province (Table 1).

Table 1. Different type properties of CEM I 42.5 R cement.

Chemical Composition of Cement (%)		Physical Parameters of Cement	
Al ₂ O ₃	5.70	Specific Gravity (g/cm ³)	3.05
Fe ₂ O ₃	2.99	Specific Surface Area (cm ² /g)	4140
SiO ₂	19.60	Fineness value over 45 µm sieve (%)	8.50
CaO	60.39	The setting time begins (hour-min)	2 s–30 min
MgO	1.90	The setting time end (hour-min)	3 s–25 min
Na ₂ O	0.15	water requirement (%)	% 29,5
K ₂ O	0.60	Volume expansion (mm)	0.5
SO ₃	2.91		
CI	0.0189	Compressive Strength (Mpa)	
s.CaO	0.34	2 days	24
Loss of ignition	7.15		
Unmeasured	0.65	28 days	52
Additive	17.87		
Total	100		

Chemical compositions of the reference limestone and different chert samples, including Toki Ferrous chert (TD), Akçakale Creek Upper Chert (AK), Toki Chert (T), Tekke Chert (TK), Gumushane Sport Ferrous Chert (GD), Akçakale Chert (AC), Besyo Chert (BC), and Gumushane Chert (GC), are provided in Table 2, while their physical properties are presented in Table 3.

Table 2. Chemical compositions and proportions of cherts.

Different Cherts	Chemical Composition of Cherts (%)								
	SiO ₂	Fe ₂ O ₃	Al ₂ O ₃	MgO	CaO	Na ₂ O	K ₂ O	SO ₃	Loss of Ignition
Limestone	3.60	0.45	1.42	19.18	29.29	0.00	0.37	0.00	42.60
TD	81.88	4.21	2.94	0.99	2.40	0.00	0.32	0.04	2.95
AK	90.54	1.88	2.41	0.09	0.66	0.10	0.42	0.00	1.38
T	83.79	0.70	0.90	1.53	3.64	0.00	0.12	0.00	5.50
TK	68.71	2.46	1.74	2.32	9.96	0.11	0.22	0.11	9.51
GD	89.19	3.22	0.37	0.00	0.30	0.00	0.00	0.00	0.16
AÇ	90.67	1.83	2.44	0.04	0.64	0.08	0.40	0.02	1.35
BÇ	54.38	0.74	0.52	6.69	14.30	0.01	0.04	0.02	10.00
GÇ	54.34	4.71	2.63	5.00	14.34	0.14	0.52	0.01	18.12

Toki Ferrous Chert (TD), Akçakale Creek Upper Chert (AK), Toki Chert (T), Tekke Chert (TK), Gumushane Sport Ferrous Chert (GD), Akçakale Chert (AÇ), Besyo Chert (BÇ), Gumushane Chert (GÇ).

Table 3. Physical properties of cherts.

Different Cherts	Fineness (%)				Specific Gravity (g/cm ³)	Specific Surface Area (cm ² /g)	Humidity Condensation (%)
	32 µm	45 µm	90 µm	200 µm			
Limestone	71.4	59.8	42.4	25.4	2.77	952	0.14
TD	58.9	23.2	3.2	0.004	2.63	4687	0.38
AK	71.5	63.9	38.6	1.4	2.64	1280	0.14
T	76.6	69.0	42.8	1.9	2.57	919	0.22
TK	69.8	61.7	38.7	1.9	2.62	1380	0.36
GD	81.7	77.6	58.4	38.2	2.61	967	0.05
AÇ	73.8	66.7	41.8	3.2	2.61	1070	0.39
BÇ	76.2	67.7	39.7	2.2	2.67	889	0.17
GÇ	76.4	68.2	48.8	5.91	2.69	1108	0.22

Toki Ferrous Chert (TD), Akçakale Creek Upper Chert (AK), Toki Chert (T), Tekke Chert (TK), Gumushane Sport Ferrous Chert (GD), Akçakale Chert (AÇ), Besyo Chert (BÇ), Gumushane Chert (GÇ).

In the study, mixture ratios for the reference sample produced only with natural limestone and mortar samples prepared according to ASTM C1260 standards with different compositions of chert samples were determined [10]. In the prepared mixture ratios, the same number of materials was used in samples produced using only limestone aggregate with reference and 8 different chert samples. Samples were prepared using 10% by weight (99 g) of No. 4 (4.75–2.36 mm) sieve, 25% by weight (247.5 g) of No. 8 (2.36–1.18 mm), No. 16 (1.18 mm–600 µm), and No. 30 (600–300 µm) sieves, and 15% by weight (148.5 g) of No. 50 (300–150 µm) sieve, according to the gradation specified in ASTM C 1260 standard. The water (206.8 g) to cement (440 g) ratio used for ASR was 0.47, and mortar mixtures were prepared. The produced mortars were placed in molds 25 × 25 × 285 mm in size and cured for 24 h at 20 ± 1 °C temperature and 50–60% relative humidity. After 24 h, the mortars were removed from the molds, and their initial lengths were measured. The samples were soaked in an 80 °C water bath for 1 day after mold removal, and their dimensions were measured. Subsequently, the samples were soaked in a 1N NaOH solution (900 mL, 40 g sodium hydroxide in distilled water) at 80 °C for 3, 7, 14, and 28 days, and periodic measurements were taken during this period.

2.2. Experiments Conducted on Materials

To determine the post-ASR elongation values of cherts with different characteristics, accelerated mortar-bar tests in accordance with ASTM C 1260 [10] standard, ultrasonic P-wave velocity measurements, and compression and flexural strength tests were conducted. Additionally, thin-section tests were performed for microstructure examinations (Figure 4).

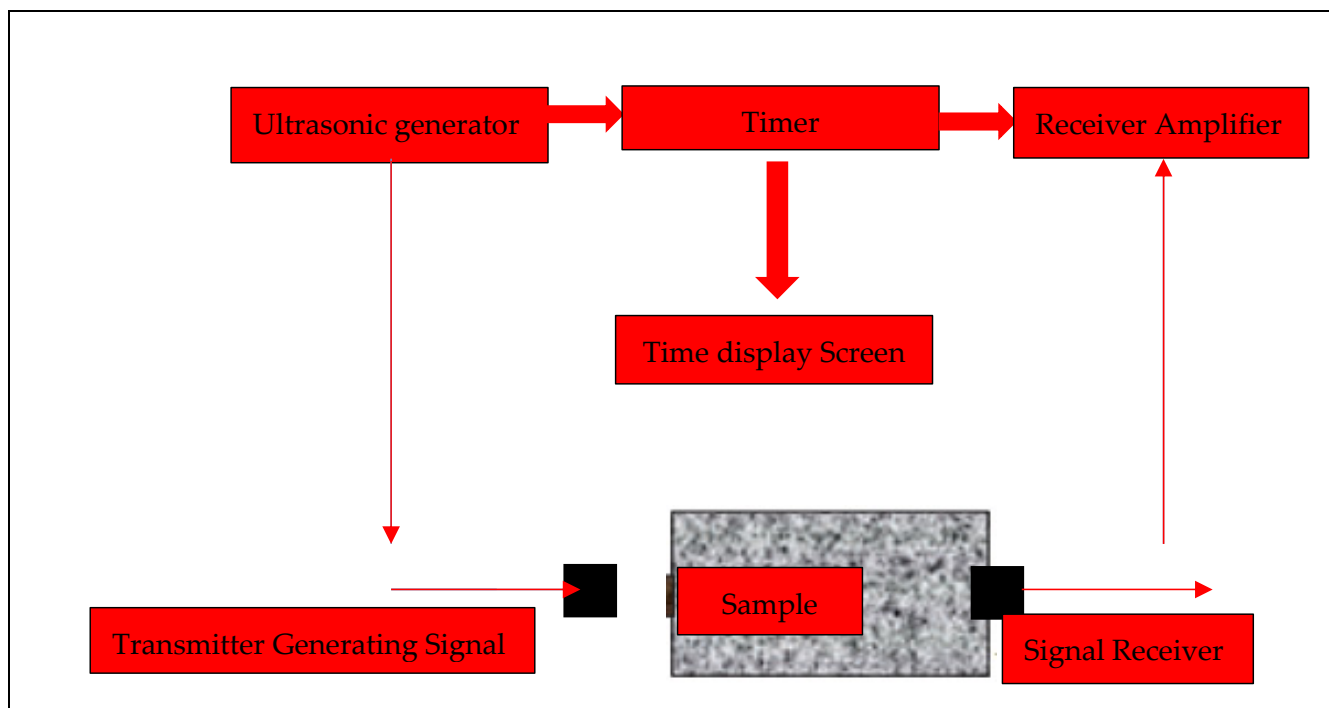


Figure 4. Ultrasonic P-wave velocity measurement setup.

The samples prepared in accordance with ASTM C 1260 standard include aggregate particle sizes from No. 4 sieve (4.75–2.36 mm) at 10% (99 g), No. 8 sieve (2.36–1.18 mm), No. 16 sieve (1.18 mm–600 μm), and No. 30 sieve (600–300 μm) at 25% (247.5 g), and No. 50 sieve (300–150 μm) at 15% (148.5 g). Prismatic samples with dimensions of 25 \times 25 \times 285 mm were prepared from these samples. Toki Ferrous Chert (TD), Akçakale Creek Upper Chert (AK), Toki Chert (T), Tekke Chert (TK), Gumushane Sport Ferrous Chert (GD), Akçakale Chert (AÇ), Besyo Chert (BÇ), Gumushane Chert (GÇ) chert samples used in the sample preparation stage were obtained using a jaw crusher. Three prism samples representing each material were prepared for measuring ASR elongation values after 3, 7, 14, and 28 days of curing. For comparison of the results, a reference sample was prepared using only limestone aggregate. The prepared prismatic concrete samples were kept in an oven at 80 ± 2.0 °C for 24 h in distilled water to measure the initial elongation values. Then, to determine the ASR elongation values of the samples at the specified curing periods, they were placed in a previously prepared ASR tank with a solution. The solution in the tank was prepared by adding 40 g of sodium hydroxide to every 900 mL of distilled water until the tank was filled, and the temperature indicator was set to 80 °C. After 3, 7, 14, and 28 days of curing, the samples were placed in the solution tank to measure the ASR elongation values. At the end of the curing periods, unit elongation values were determined using an ASR extensometer. The obtained elongation values were used to calculate unit elongation values as a percentage (Equation (8)).

$$\% L = (\Delta LL) \times 100 \quad (8)$$

In Equation (8),

% L = Percentage change in height;
 ΔL = For example, change in height (mm);
 L = Indicates the initial length of the sample (mm).

After measuring the ASR elongation percentage results following the test, it was determined that when the elongation limit value after the 14-day curing period specified in ASTM C 1260 standard is $\leq 0.10\%$, the aggregate used is nonreactive and can be used as a harmless aggregate in terms of ASR in concrete. However, if the ASR elongation value is between 0.10% and 0.20%, it is considered suspicious in terms of ASR development, and when the limit value is $\geq 0.20\%$, it indicates that the aggregate will create reactivity in terms of ASR (ASTM C 1260, 2014).

2.2.1. Microstructural Examination of Chert Samples with Different Compositions for ASR Development

After measuring the ASR elongation values of concrete samples prepared with cherts of different compositions and properties following the 28-day curing period, the mechanism and structural characteristics of ASR formation were determined under a petrographic microscope.

2.2.2. Examination of Mechanical Properties after ASR Development in Chert Samples with Different Compositions

ASR elongation values were measured for samples produced using different chert samples after curing periods of 3, 7, 14, and 28 days. Following the measured values, mechanical properties were revealed through ultrasonic P-wave velocity, flexural, and compressive strength tests.

2.2.3. Ultrasonic-P Wave Velocity Test

The ultrasonic velocity measurement on the prepared concrete samples was determined according to ASTM C597 [66]. Ultrasonic velocity measurement was applied to concrete samples with cherts, and the operating principle of the device is provided in Figure 4. The device operates on the principle of measuring the propagation speed of the wave in the medium based on the reactions received by the receiver and transmitter sensors. The ultrasonic wave velocity test was applied to $25 \times 25 \times 285$ mm prismatic samples. The samples were placed horizontally in the device for wave velocity measurement. Each sample was divided into three sections, and measurements were made for each section. These sections were divided into upper, middle, and lower, and three measurement values were taken for each section. The average of these 3 values reflecting the sample was calculated to obtain the result. During the measurement, the device's heads were designed to be in the same line and parallel to each other in the horizontal position of the sample. The sample heads were placed in a way that did not create gaps in the sample during the measurement, and the results obtained were calculated according to Equation (9).

$$V = (S/t) \quad (9)$$

In the given equation,

V = Ultrasonic wave velocity (m/s);

S = Length (length) of the sample (m);

t = The time (s) it takes for an ultrasonic wave to travel from one surface to another, (microseconds).

2.2.4. Uniaxial Compression Strength Test

After determining the ASR length measurement values for the prepared 3 samples with dimensions of $25 \times 25 \times 285$ mm at 3, 7, 14, and 28 days of curing, a flexural test was conducted by first splitting them in half. Three samples were divided into two equal parts, resulting in six specimens. A compressive strength test according to the TS EN

196-1 [67] standard was applied to each specimen. After placing $40 \times 40 \times 40$ mm-sized metal crushing heads on the lower and upper surfaces of each specimen, a compressive test was conducted. The arithmetic average of the obtained results from the 6 tests was taken, and the uniaxial compressive strength values were determined by dividing the measured breaking force (F) in the device by the cross-sectional area of the specimen, as given in Equation (10).

$$f_c = \frac{F}{A_C} \quad (10)$$

In the equality,

f_c = Compressive strength, MPa (N/mm^2);

F = Maximum load reached at fracture, N;

A_C = The cross-sectional area (mm^2) of the specimen on which the pressure is applied.

2.2.5. Flexural Strength Test

Flexural strength tests were conducted on the cork samples with different components subjected to ASR. The test was carried out using a concrete press with a capacity of 200 tons and a loading speed of 50 N/s according to the TS EN 196-1 [67] standard. The samples, which had been completed during periods of 3, 7, 14, and 28 days and had measured ASR elongation values, were used for the tests. The prepared prismatic specimens were placed in the flexural apparatus, and loading was initiated. Due to the effect of the applied force (P) during loading, the specimens were split in half. The obtained measurement values were used to calculate the unknowns in Equation (11), and the flexural strength values were determined.

$$R_f = \frac{1.5 \times F_f \times I}{b^3} \quad (11)$$

In the equality,

R_f : Flexural strength, Newton/mm (MPa);

F_f : The force applied to the center of the prism at the moment of fracture (Newton);

b: The length of the side of the cross section of the prism (mm);

I: Distance between support cylinders (mm).

The materials used in the study, sample production stages, measurement of unit elongation, petrographic microscope images applied to the obtained data, ultrasonic P-wave velocity, and flexural and compressive strength tests are illustrated in a flowchart, which is presented in Figure 5.

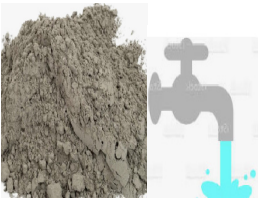
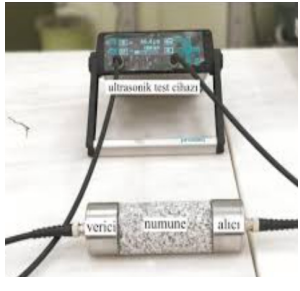
<p>CEM I 42.5 R CEMENT AND TAP WATER</p>	<p>LIMESTONE AGGREGATE IN DIFFERENT SIZES</p>	<p>DIFFERENT CHEMICAL COMPONENTS CHERT AGGREGATE</p>	<div style="border: 1px solid black; padding: 10px; text-align: center;"> <p>STAGE 1</p> <p>PREPARATION OF MATERIALS</p> </div>
			
<p>SIZE REDUCTION AND SCREENING IN JAW CRUSHER ACCORDING TO ASTM C1260</p>	<p>PREPARATION OF MIXTURE</p>	<p>SAMPLE PRODUCTION (25X25X285 MM)</p>	<div style="border: 1px solid black; padding: 10px; text-align: center;"> <p>STAGE 2</p> <p>SAMPLE PRODUCTION</p> </div>
			
<p>SAMPLES FOR THE FIRST SIZE CHANGE. HOLDING IN THE OVEN AT 80 ±2 °C</p>	<p>HOLDING SAMPLE IN THE ASR TANK TO DETERMINE 3, 7, 14 AND 28 DAY CURE TIME LENGTH CHANGE VALUES</p>	<p>MEASUREMENT OF ASR LENGTH CHANGE VALUES OF SAMPLES WITH CURING TIME</p>	<div style="border: 1px solid black; padding: 10px; text-align: center;"> <p>STAGE 3</p> <p>ASR MEASUREMENT EQUIPMENT</p> </div>
			
<p>3, 7, 14 AND 28 DAYS COMPRESSION AND TENSILE STRENGTH OF SAMPLES</p>	<p>ULTRASONIC-P WAVE SPEED</p>	<p>THIN SECTION INVESTIGATIONS</p>	<div style="border: 1px solid black; padding: 10px; text-align: center;"> <p>STAGE 4</p> <p>MECHANICAL AND MICRO EXAMINATIONS AFTER ASR</p> </div>
			

Figure 5. ASR measurement, mechanical and microstructure investigations in concretes produced using cherts.

3. Results and Discussion

3.1. The ASR Elongation Values of Chert Samples with Different Chemical Compositions

In the conducted study, the elongation values for samples produced using limestone and eight different chert specimens for 3, 7, 14, and 28 days are presented in Figures 6–8. Assessments based on different limits according to ASTM C 1260 standards are made on the figures. The limit values specified in the standard are given in Table 4, and the comparison of the results is given in Table 5.

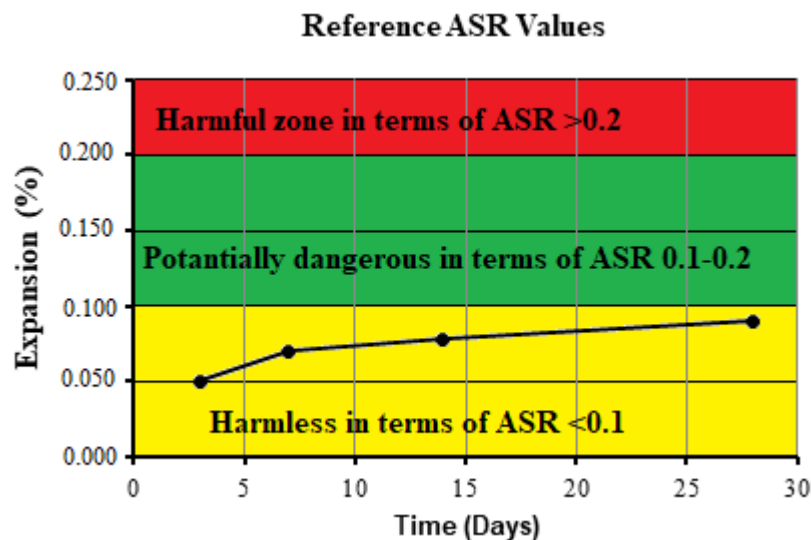


Figure 6. Reference sample ASR expansion change values.

Table 4. ASR extension limit values according to ASTM C 1260 standard.

ASR Expansion Change Values (%)	<0.1	0.1–0.2	>0.2
Determination by ASR length change method after 14 days of curing period	It is harmless in terms of ASR.	It is necessary to measure again after the 28th day, although it may be harmful. May be potentially dangerous	Harmful zone in terms of ASR

Table 5. Expansion change values of mortar bars ASR 3, 7, 14, and 28 days.

Chert Types	ASR Expansion Change Values (Day)			
	3	7	14	28
R	0.0500	0.07000	0.07800	0.09000
TD	0.0349	0.04421	0.04579	0.06211
AK	0.0754	0.09895	0.12175	0.25439
T	0.0153	0.05351	0.07947	0.19000
TK	0.0447	0.13596	0.51018	0.51667
GD	0.0065	0.18246	0.27842	0.40561
AÇ	0.2301	0.29049	0.32102	0.38067
BÇ	0.0292	0.16956	0.37921	0.41447
GÇ	0.1350	0.30151	0.33449	0.35256

Reference (R), Toki Ferrous Chert (TD), Akçakale Creek Upper Chert (AK), Toki Chert (T), Tekke Chert (TK), Gumushane Sport Ferrous Chert (GD), Akçakale Chert (AÇ), Besyo Chert (BÇ), Gumushane Chert (GÇ).

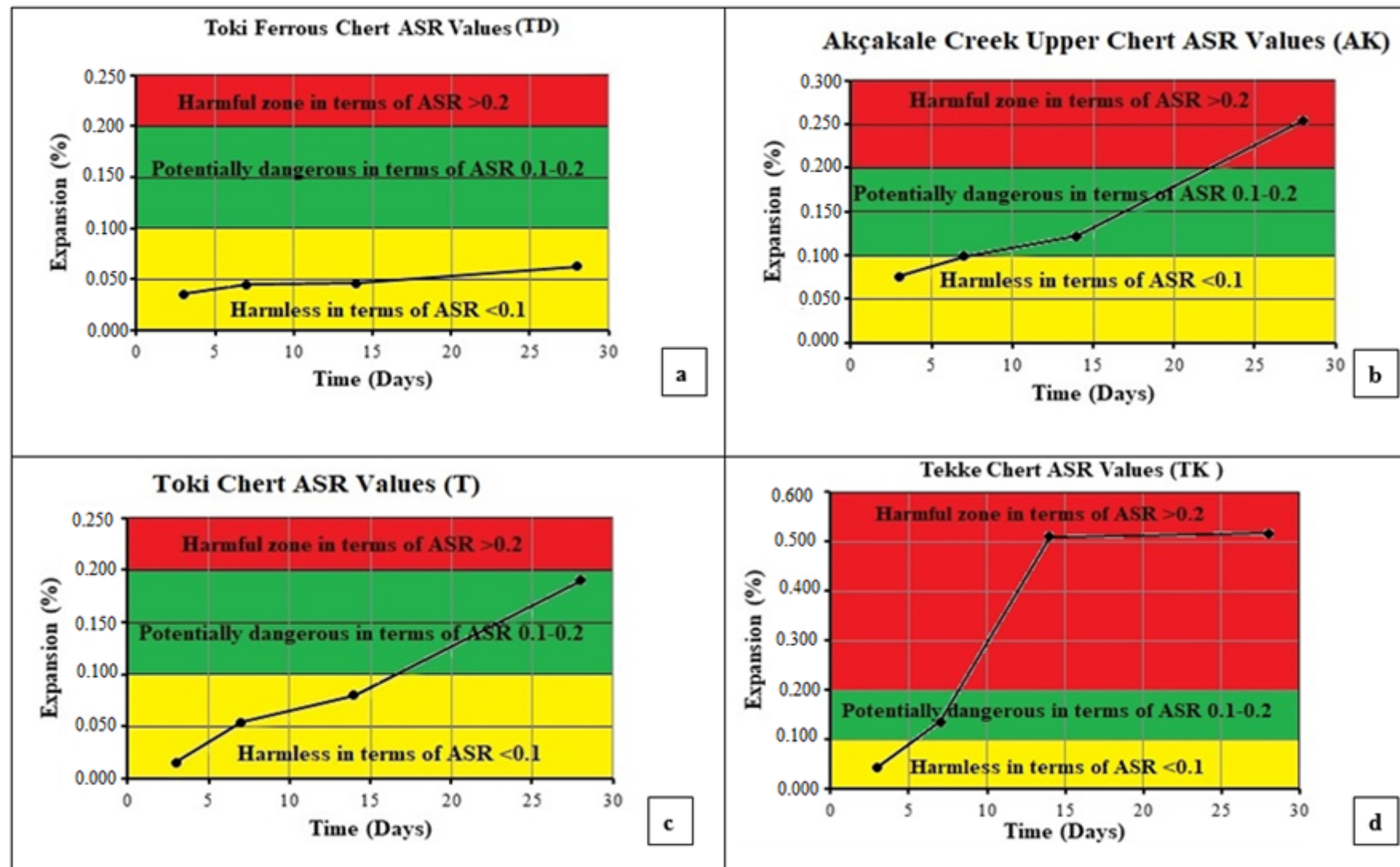


Figure 7. ASR expansion change values of different chert samples (a) Toki Ferrous chert (TD), (b) Akçakale Creek Upper chert (AK), (c) Toki chert (T), (d) Tekke chert (TK).

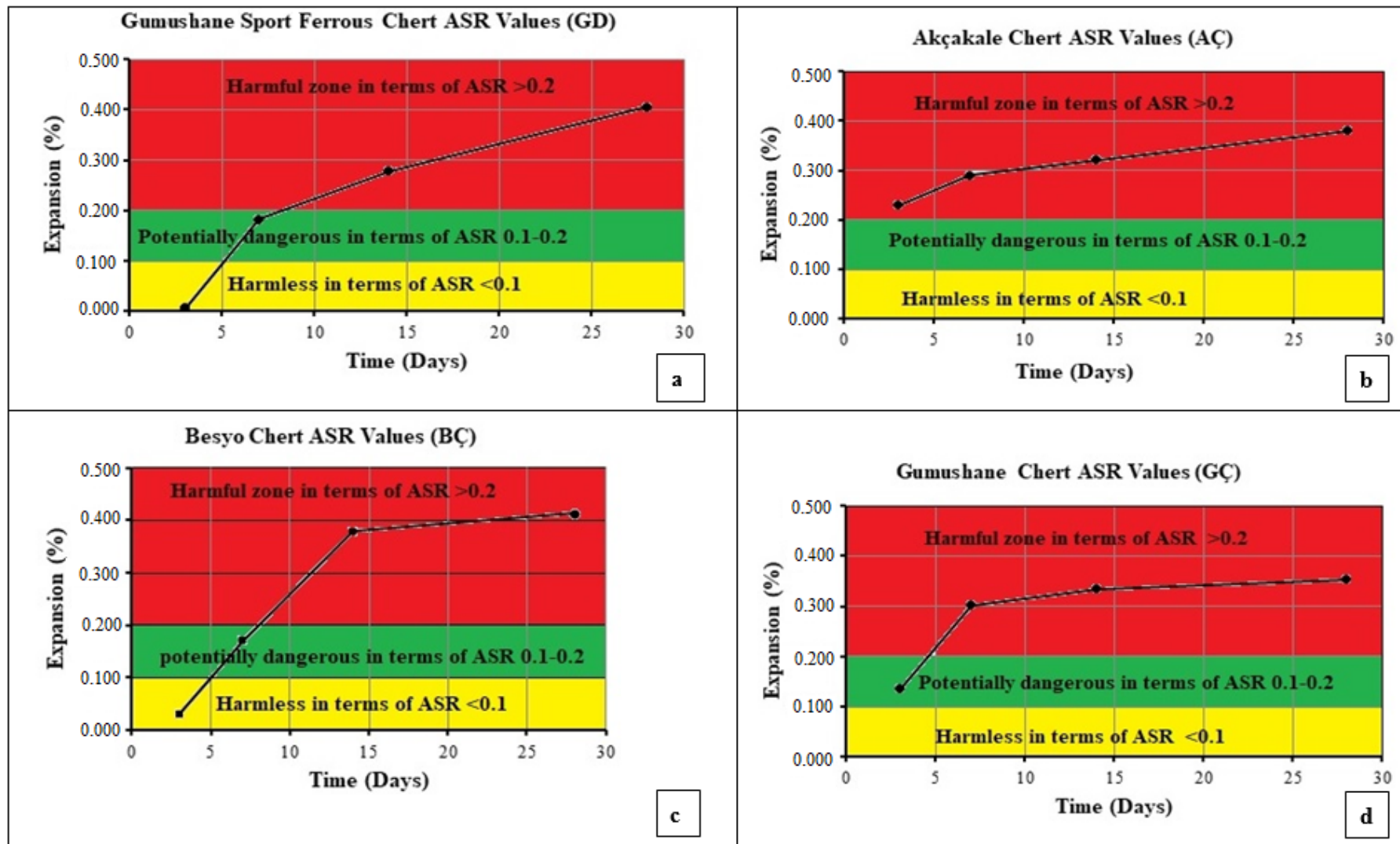


Figure 8. ASR expansion change values of different chert samples (a) Gumushane Sport Ferrous chert (GD), (b) Akcakale chert (AC), (c) Besyo chert (BC), (d) Gumushane chert (GC).

As a result of the study, the ASR elongation values of the reference and different chert samples are presented together in Figure 9. According to the obtained results, the ASR elongation values for the reference limestone aggregate increased after 3, 7, 14, and 28 days of curing. However, as the values remained below the threshold specified in ASTM C 1260 (<0.1), it was determined to be a nondamaging aggregate. Among the chert samples used in the study, the Toki Ferrous Chert (TD) and Toki Chert (T) samples also exhibited elongation values below the specified threshold, making them acceptable as nondamaging aggregates in terms of ASR development. However, other chert samples, including Akçakale Creek Upper Chert (AK), Tekke Chert (TK), Gumushane Sport Ferrous Chert (GD), Akcakale Chert (AC), Besyo Chert (BC), and Gumushane Chert (GC), showed elongation values above the threshold after the 14-day curing period. Following the 28-day curing period, the elongation values exceeded 0.2, indicating potential harm due to ASR development, and these aggregates were considered harmful.

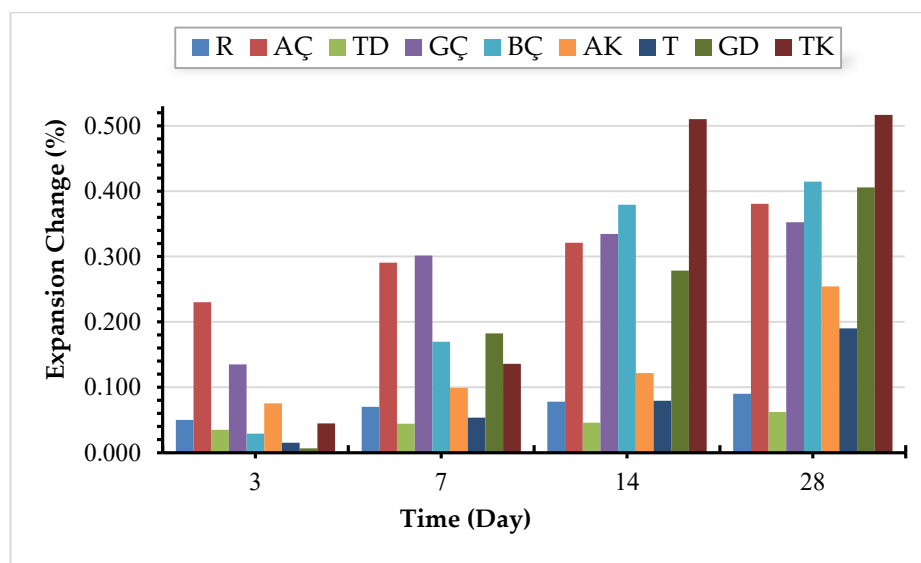


Figure 9. Results showing ASR expansion change values of reference and different chert samples.

The development of alkaline silica reaction in the AK, TK, GD, AÇ, BÇ, and GÇ chert samples used in the study was due to the presence of reactive silica, pore solution with high alkalinity and moisture in the environment. In addition, the texture difference of reactive silica, crystal structure, decreasing cooling rate during the rock formation process, silica minerals in the aggregate, amorphous or glassy structure or cryptocrystalline, crystalline and microcrystalline structure during the rock formation process, alkali content from cement and concrete, different Blaine fineness values, and the shape of the aggregates caused different elongation values of the chert samples after ASR. The reactive properties of the quartz mineral in the composition of cherts led to the development of ASR in the samples used [67]. In the studies conducted, cherts are ranked fourth in terms of forming ASR. The cherts used in this study also develop reactive silica-containing ASR. However, while ASR developed in five of eight different chert samples with reactive silica content and had height elongation values above the limit values specified in the standards, this situation did not develop in three cherts. In addition, the decrease in one of the components forming ASR causes the reaction formation to decrease or stop. However, in this study, we see that in cherts that developed ASR, the reactive silica content was sufficient until the 28-day cure period and the height growth values continued to increase.

In the studies, cherts have been accepted as a mineral showing reactivity. In addition to these, amorphous silica, opal, unstable crystalline silica, chert, chalcedony, other cryptocrystalline forms of silica, metamorphically weathered and degraded quartz, deformed quartz, semi-crystallized quartz, and pure quartz are listed according to the degree of decrease in

reactivity. It is inevitable that aggregates consisting of these components will develop ASR, and chert has taken its place among the minerals with these components and gave results supporting previous studies by creating reaction. One of the components that enables the formation of alkaline silica reaction is the alkali equivalent amount used in concrete or cement expressed as sodium oxide equivalent amount. This value was calculated for all chert samples used in the study and the values obtained were evaluated in terms of ASR development (Equation (12)) (TS EN 196-2) [68].

$$(\text{Na}_2\text{O})_{\text{eşd}} = \text{Na}_2\text{O} + 0.658 \times \text{K}_2\text{O} \quad (12)$$

The alkali equivalent amount for the limestone aggregate and eight chert samples in cement is given in Table 6.

Table 6. Alkali equivalent amounts of cement, reference, and chert.

Sample Types	$\text{Na}_2\text{O} + 0.658 \times \text{K}_2\text{O}$ (%)	SiO_2 (%)	Blaine (cm^2/g)	Humidity, %
Çimento	0.5448	19.60	4140	0.12
R	0.24346	3.60	952	0.14
TD	0.21056	81.88	4687	0.38
AK	0.37636	90.54	1280	0.14
T	0.07896	83.79	919	0.22
TK	0.25476	68.71	1380	0.96
GD	0	89.19	967	0.05
AÇ	0.3432	90.67	1070	0.39
BÇ	0.03632	54.38	889	0.17
GÇ	0.48216	84.34	1108	0.22

Reference (R), Toki Ferrous chert (TD), Akçakale Creek Upper chert (AK), Toki chert (T), Tekke chert (TK), Gumushane Sport Ferrous chert (GD), Akçakale chert (AÇ), Besyo chert (BÇ), Gumushane chert (GÇ).

Table 6 calculates the alkali equivalent amounts causing alkali–silica reactions (ASR). The ASTM C 150 [69] standard considers a threshold value of 0.6%. The alkali values for all samples used in the study were below the specified limit in the standard, indicating nonharmful properties regarding alkali content. Cherts labeled Toki Ferrous Chert (TD) and Toki Chert (T) were not considered harmful aggregates for ASR development, unlike other cherts used in the study, including Akçakale Creek Upper Chert (AK), Tekke Chert (TK), Gumushane Sport Ferrous Chert (GD), Akcakale Chert (AC), Besyo Chert (BC), and Gumushane Chert (GC), which exhibited harmful effects in terms of ASR development due to different factors. In particular, the amount of CaO in the expanding chert aggregates showed a supportive effect on ASR formation by bringing together different components. The absence of ASR in the chert samples symbolized as TD and T in the study reflects the possibility of low values in terms of CaO composition. However, in the study, this is due to the presence of cherts with a lower value than the CaO composition in the composition of the mentioned cherts and the presence of a high reactive silica component in case of ASR formation. Wang and Gillot (1992) [70] demonstrated in their study that calcium–alkali–silica gel exhibits non-swelling characteristics. However, the Ca ions coming from the abundant CaO component in the environment replace the alkalis in ASR, allowing these components to be released into the environment. Although eight different chert bands all showed reactive properties, their ASR formation potential differed depending on their expansion values. In the studies, it has been observed that swelling reaches maximum levels when the opaline, which is accepted as reactive, is 3–5%, and if this ratio is more than 20%, no swelling is observed. The reason for the absence of swelling despite the excess of reactive minerals is firstly perceived as an unacceptable situation. This situation has arisen from the insufficient presence of all active silica in the aggregate due to the

inadequate alkali oxides and the ineffectiveness of containing alkali silica gel [71]. Despite the high silica content in the aggregates referred to as TD and T in the study, the reason for the low expansion is that the alkalis present in the environment are not sufficient to react with all the excess silica. The lack of sufficient components has prevented the reaction from taking place fully [72]. The differences in ASR expansion values are also attributed to their different Blaine fineness values. Grinding finer materials during the milling process has led to smaller particles having a lower degree of structural order and unstable silica minerals compared to larger aggregates. The inverse relationship between particle size and surface area of smaller aggregates has increased the chances of attack [73]. Therefore, the increase in specific surface area of reactive aggregates has contributed to an increase in ASR expansion as particle size decreases [37,38]. The variations in ASR expansion values of mortar samples have depended on several factors. These factors include the reactivity degree of the aggregate, the chemical and mineral composition within the aggregate, crystallinity, amorphous structure, the solubility degree of amorphous silicate in the alkali pore solution, and the sensitivity of the aggregate to ASR [27]. In many studies, well-known aggregates are mostly sensitive to ASR and are classified based on their amorphous and crystalline structures. Mortar has been considered a reactive aggregate [74]. Rocks, such as opal, tridymite, cristobalite, acid volcanic glass, and basalt, that do not contain a crystal structure and exhibit an amorphous structure are irregular, internally contain microcracks, and create channels for many cage defects to easily penetrate, making them reactive [18].

The degree of porosity in aggregate particles is crucial for ASR formation. The varying composition of silica within the aggregates has led to the formation of different expansion values due to differences in texture and crystal structure. The formation of aggregates has resulted in samples with different forms and characteristics, depending on the cooling rate during the formation of silica rock, ultimately resulting in different expansion values. The silica minerals in aggregates exist in various forms such as amorphous or glassy phase (non-crystalline), cryptocrystalline, microcrystalline, and crystalline phases, depending on the decreasing cooling rate, and the formation of quartz crystals leads to variations in the expansion values of the aggregates due to the stress during crystal formation [75].

Aggregates containing strained quartz are also prone to reactivity. Cristobalite and tridymite, found in crystalline form at high temperatures and crystallizing as a result of rapid cooling, are unstable at normal temperatures. Cherts containing these crystals are reactive. Opal, an amorphous form of silica containing variable amounts of water, is highly reactive [25,32]. Additionally, it is in a direct relationship with the reactive surface area. As a result, reactive silica can be easily transferred to a larger surface area, leading to the formation of more ASR. For example, Thomas et al. (2013) [76] compared the structure of quartz (nonreactive aggregate type) with opal structure (reactive aggregate type). Quartz has a completely crystalline structure with each silicon tetrahedron bonded to oxygen ions. Each oxygen ion is bonded to two silicon ions to achieve electrical neutrality. The opal structure, despite having a crypto-crystalline and amorphous silica with each silicon tetrahedron not present, binds and dissolves oxygen ions, making them unstable [49]. In the presence of ASR, hydroxyl ions in the pore solutions penetrate silica particles, loosening the cage structure. Therefore, in crypto-crystalline or amorphous silica (such as opal), this cage structure easily breaks down with the entry of hydroxyl ions, making the aggregates susceptible to ASR. In contrast, well-crystallized silica is not sensitive to ASR attacks due to its regular cage structure and oxygen ions bonded to each silicon. Poorly crystallized, heavily cage-defective, amorphous, glassy, and microporous aggregates have shown more susceptibility to ASR formation [32].

The different Blaine fineness values of the cherts also contributed to variations in ASR elongation values because micro-cracks within aggregates affect the reaction surface area. The particle size of aggregates being fine or coarse has different implications for ASR formation. Some researchers have argued that a certain size of expansion occurs at maximum levels (0.07–0.85 mm), and particles larger and smaller than this size reduce expansion [77]. Mehta (1993) [41] and SHRP (2003) [78] emphasized in his study that the

particle size for the maximum expansion caused by reactive aggregates is between 1 and 5 mm. The differences in reactivity of the chert aggregates used in the study could be attributed to different Blaine fineness values, as well as different alkali, silica, and calcium content. Nishibayashi and Yamura (1992) [79] and Ramyer et al. (2005) [44] determined in their research that the initial expansion of concrete occurs when only fine and reactive aggregates are used, stabilizing later. Similarly, using only reactive coarse aggregate leads to slow and prolonged expansions. The dimensional differences of aggregates have different effects on ASR. Fine aggregate size is more sensitive to ASR formation compared to coarse aggregate [32,35]. This is because smaller particles during the grinding process have more unstable minerals and lower structural defects compared to larger particles [72,78].

3.2. Microstructural Impact of Chert Samples with Different Compositions on Alkali–Silica Reaction (ASR)

For the alkali–silica reaction (ASR) to occur, certain mineralogical components must be present. The determination of these components is carried out using the ASTM C295 [9] standard, titled “Standard Test Method for Petrographic Analysis of Aggregates”. In the method, samples causing ASR are examined under a petrographic microscope, and the formations are presented in Figure 10. The polarizing microscope images in Figure 10 were obtained with double nicol and objective lens magnification ratios of 4×0.10 . Following the microscopic examinations, ASR formations, mineralogical compositions, and details are provided in Table 7. Particle characteristics, such as shape, size, texture, color, mineral composition, and physical conditions observed in thin sections under the petrographic microscope, are classified according to mineralogical compositions, texture, formal properties, and ASR formations expressed in the ASTM C295 [9] standard [80].

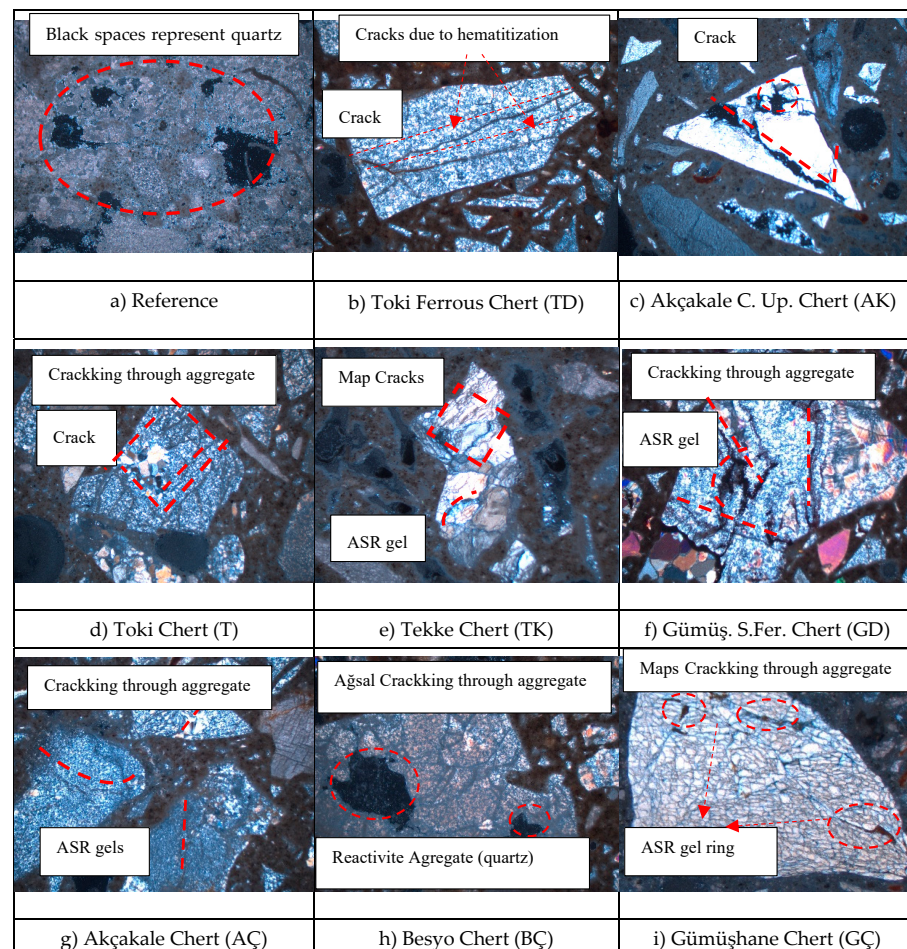


Figure 10. Alkali silica reaction thin-section images.

Table 7. Petrographic analysis results of cherts.

Samples	Description	ASTM C295 Petrographic Classification of ASR
Reference (R)	Black voids are quartz, and pink voids are sericite and clay. It does not form ASR.	CLASS I
Toki Ferrous Chert (TD)	The cracks in the aggregate are due to haematitisation from the iron mineral in the chert and do not cause ASR	CLASS I
Akçakale Creek Upper Chert (AK)	The triangular grain is composed of amorphous quartz, and the cracks on it are due to ASR.	CLASS III
Toki Chert (T)	There is secondary quartz formation and hematitisation. The cracks, which were initially due to hematitisation, were later formed as a result of ASR and manifested themselves by taking a map image.	CLASS II
Tekke Chert (TK)	Cracks due to ASR were intensively formed on the aggregate, and these showed themselves in the map appearance.	CLASS III
Gumushane Sport Ferrous Chert (GD)	There are ASR gels formed around the aggregate and map cracks surrounding its interior	CLASS III
Akçakale Chert (AÇ)	It contains chalcedony. ASR gels and network-like cracks were formed around and inside the aggregate grains.	CLASS III
Besyo Chert (BÇ)	There are two different quartz grains in the aggregate and a network structure formed due to ASR.	CLASS III
Gumushane Chert (GÇ)	The aggregate is composed of quartz grains. The quartz is dominated by intermittent ASR gel formations and network crack structure.	CLASS III

CLASS I: Far from showing alkaline reactivity, CLASS II: Alkali reactivity uncertain, CLASS III: May show alkali reactivity.

Binal (2004) [81] determined the alkali reactivities of five different reactive aggregates, namely opal nodule, chert, chalcedony nodule, andesite, and basalt, in terms of their petrographic, mechanical, and physical properties. Petrographically, different alkali–silica gel developments were identified under the microscope based on the types of reactive aggregates. The development of alkali–silica gel in these aggregates was determined with different structural images under the microscope, including halo-shaped formations in opal minerals, concentric halo formations along radial cracks, and radial fibrous alkali–silica gel images in chert minerals due to the aggregate being composed of fibrous cryptocrystalline quartz. Additionally, alkali–silica gel images, in the form of radial fibers originating from the aggregate, were observed in chalcedony minerals. The results obtained correspond with the elongation results, reflecting the correlation between petrographic analysis and ASR formation mechanisms. It should be noted that, while petrographic analysis results are considered in this study and in previous research, they are utilized as an auxiliary method, and the ASR formation mechanism is not determined solely based on petrographic analysis. According to the British Specification for Highway Works, a material is considered nondetrimental if it is not contaminated by reactive silica minerals, such as opal, tridymite, and cristobalite, and if it does not contain more than 2% by mass of chert, flint, or chalcedony. Quartz should not contain more than 30% by mass of metamorphosed quartzite. Petrographic analyses in this study were supported by the elongation results to determine minerals causing ASR.

In Figure 10, the structure of mineralogical components causing ASR, as well as the condition of the aggregate and pore structure, have significantly contributed to the initiation and propagation of the alkali–silica reaction. The porosity of the aggregate is an effective factor in ASR. A higher porosity structure has made the concrete and aggregate more sensitive to ASR, i.e., it has increased its susceptibility [27,34]. The porous structure of both concrete and aggregate with high porosity easily absorbs the moisture causing ASR, facilitating the transport of different components. The rapid spread of alkali ions in porous aggregate initiates the dissolution of the aggregate causing ASR [37]. In the

study conducted by Eker et al. (2023) [82], they examined the effect of the fineness of fly ash on the ASR formation mechanism. They compared the microstructural changes of the reactive reference aggregate causing ASR with samples containing fly ash. The ASR in the reference concrete had the highest elongation value, as observed in the images obtained; there were cracks in the macrostructure, ASR gel formation inside the aggregate, and large and small cracks around or along the aggregate. The reducing effect of fly ash fineness and replacement ratio on ASR was attempted to be demonstrated through petrographic analyses. According to the obtained images, increases in the fineness of fly ash and replacement ratio led to decreases in voids and crack structures. After petrographic examination, the absence of ASR in the chert samples symbolized as R, TD, and T is due to the lack of structures and minerals that will form ASR in terms of crystal structure. In addition, the absence of fractures and cracks in the cherts, as well as the mineral structure, caused products that would form ASR to enter the aggregate, and no reaction developed.

3.3. Examination of Mechanical Properties of Chert Samples in Different Compositions of Aggregates following ASR Development

Ultrasonic P-Wave Velocity

After measuring the ASR elongation values of the samples following the 28-day curing period, ultrasonic P-wave velocity and flexural and compressive strength tests were conducted. All the results of the experiments are presented in Table 8. Figures 11–13 depict the mechanical data for the samples.

Table 8. At the end of 28-day curing period, all mechanical results of the specimens.

Sample Names									Experiments
R	AK	TD	GÇ	BÇ	AÇ	T	TK	GD	
3683	3674	3685	3391	3300	3427	3782	3253	3557	Ultrasonic Wave Velocity (m/sn)
9.32	5.17	9.71	3.05	2.93	4.31	9.14	2.76	4.29	Compressive Strength (MPa)
2.77	2.44	2.83	2.24	2.18	2.33	2.84	1.98	2.40	Flexural Strength (MPa)

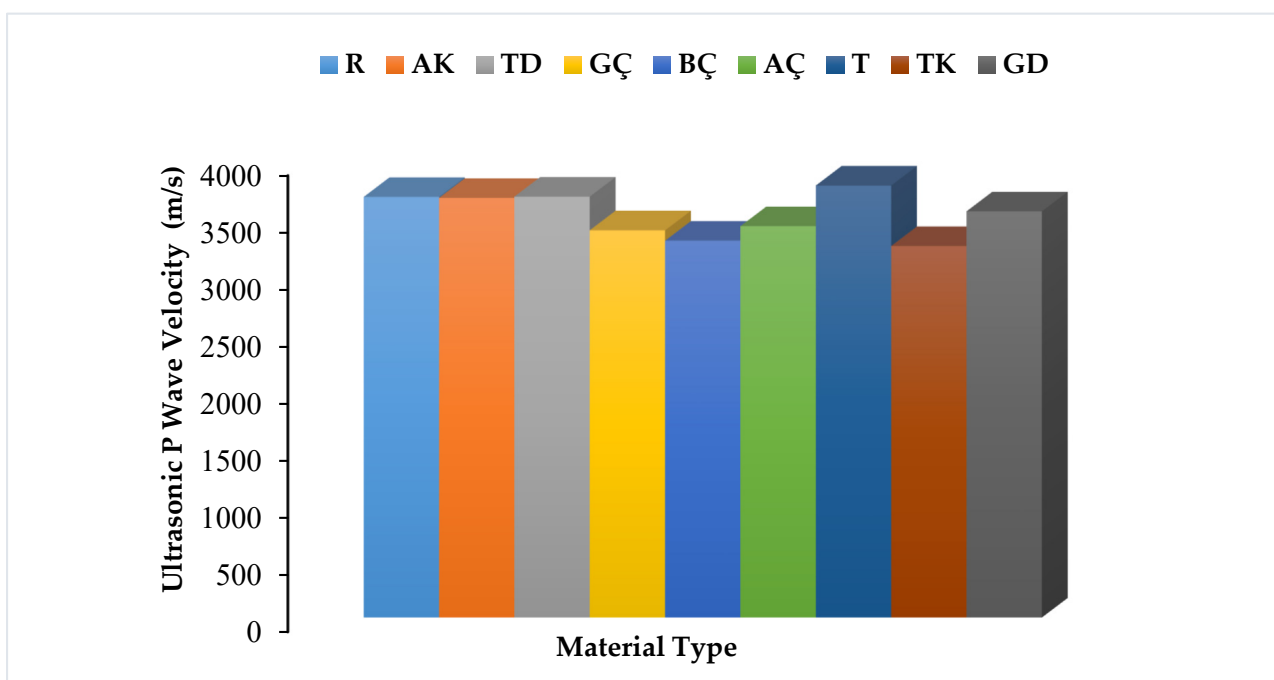


Figure 11. Ultrasonic P-wave velocity results for chert samples.

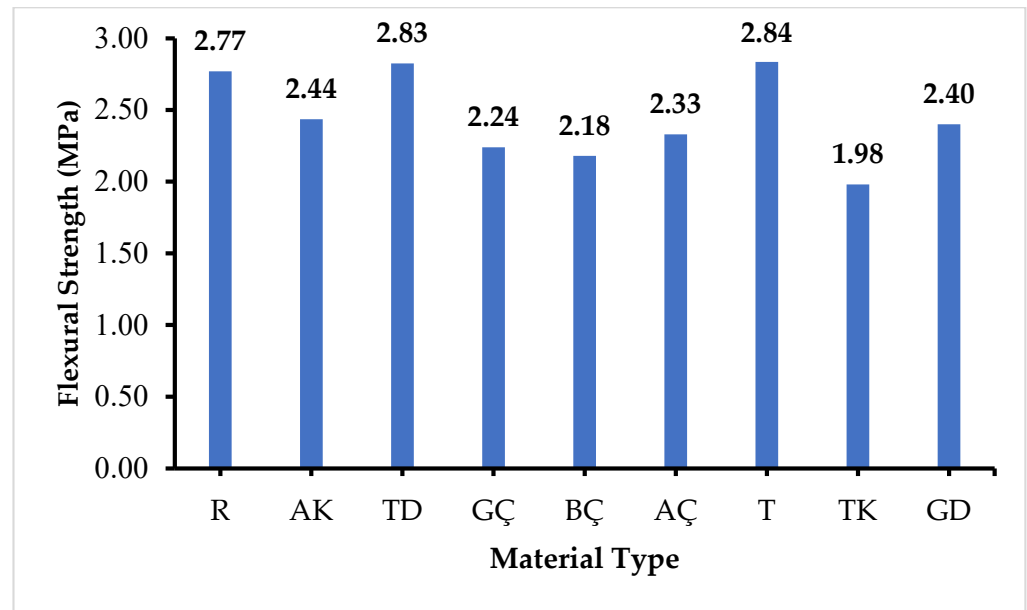


Figure 12. Flexural strength value results of chert specimens.

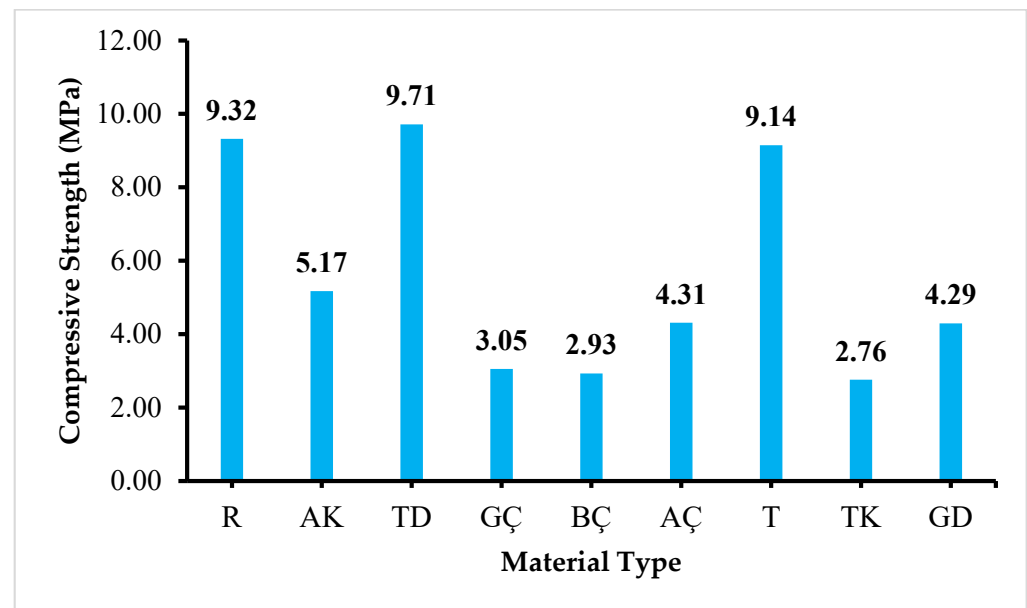


Figure 13. Compressive strength value results of chert specimens.

After ASR, the sample with the highest elongation value had the lowest ultrasonic wave velocity value, while the sample with the lowest elongation had the highest ultrasonic wave velocity value. Following a 14-day curing period, the highest ultrasonic P-wave velocity of 3685 m/s was determined for the TD mortar sample with the lowest ASR elongation value, while the highest ASR elongation value belonged to the TK sample with the lowest ultrasonic P-wave velocity of 3253 m/s (Figure 11).

The ultrasonic P-wave velocity results of the aggregates used in the study were compared in Table 9 in terms of concrete quality, as per the studies conducted by [83,84].

Table 9. Evaluation of ultrasonic P-wave velocity values in terms of concrete quality.

Ultrasonic P-Wave Velocity (m/sn)	Concrete Quality	
	Whitehurst, 1951 [82]	Uyanık et al., 2011 [83]
Excellent	>4500	>4565
Good	3650–4500	3515–4565
Medium	3050–3650	2930–3515
Poor	2000–3050	2110–2930
Very Poor	<3000	<2110

The samples represented by symbols T, TD, R, and AK, when used as aggregates in concrete, result in high-quality concrete, while concrete produced with the samples represented by symbols GD, AC, GC, BC, BK, and TK exhibit medium-quality characteristics. After ASR, there was no significant decrease observed in ultrasonic P-wave velocities. It is indicated that the changes in ultrasonic P-wave velocity values are influenced by the mineralogical compositions within the aggregate, but this influence leads to relatively lower variations compared to microcrack structures [45].

4. Flexural Strength Test Results

To determine the mechanical strength losses in mortar samples prepared using chert samples after the ASR effect, flexural and compressive tests were conducted on samples aged for 28 days under water curing, and the obtained flexural strength values are presented in Figure 12.

The flexural strength values of the samples exhibited elongation in their lengths and mechanically manifested themselves by obtaining low flexural strength values after exposure to ASR. As the elongation value increased after ASR, a decrease in flexural strength values was observed. Among the cherts symbolized as R, TD, and T, which did not induce ASR according to standards, the highest flexural strength values were obtained. For the remaining samples symbolized as AK, GD, AC, GC, BC, and TK, a decrease in elongation values corresponded to an increase in flexural strength values. The highest flexural strength value was 2.84 MPa for the sample symbolized as T, while the lowest flexural strength value was 1.98 MPa for the sample symbolized as TK. The difference between the highest and lowest flexural strength was 0.86 MPa, representing a strength loss of 30.28%. Demir (2010) [85] determined flexural strength values in mortar samples prepared with the addition of silica fume and fly ash after ASR. It was found that the flexural strength values of the silica fume were 18% better than those of the fly ash-added samples. When reactive aggregate is used in concrete, it has been concluded that it has significant effects on guiding properties such as flexural and compressive strength values. Studies have shown that after the ASR development of mortar samples, concrete flexural/tensile and elastic modulus are affected [86]. The flexural strength values obtained for the mortar samples have yielded very close results. This indicates that flexural strength values may not always change at the same rate and speed. The crack structure and formations developed in mortars after ASR, along with other mechanisms contributing to the mineral composition inside the aggregate and ASR formation, easily affect the flexural strength values [25,45,87].

Compressive Strength Test Results

After determining the ASR length measurement values of mortar samples that completed the 28-day curing period, flexural strength was measured, followed by the determination of compressive strength values. The obtained results are presented in Figure 13.

A decrease in compressive strength values was observed after ASR. The decrease was more pronounced in the sample with the highest elongation value due to ASR. The compressive strength values, from highest to lowest, were ranked as TD, R, and T for samples without ASR, and as AK, GD, AC, GC, BC, and TK for samples with ASR. The

percentage loss of pressure values between samples, from highest to lowest, is given in Table 10.

Table 10. Compressive loss due to ASR between chert specimens.

Compressive Loss Values between the Four Specimens after ASR (%)							
TD-R	R-T	T-AK	AK-GD	AÇ-GD	AÇ-GÇ	GÇ-BÇ	BÇ-TK
4.02	1.93	43.44	17.02	0.46	29.24	3.94	5.81

Among the chert samples, the highest compressive strength value belonged to the TD sample, with a value of 9.71 MPa, while the lowest compressive strength value for the TK sample was calculated as 2.76 MPa. The pressure loss between the two chert samples was 6.95 MPa. A pressure loss of 71.6% was determined between the TD sample without ASR and the TK sample with the highest elongation value due to ASR. Deformation structures formed in the samples were supported by pressure and flexural strength losses. In his study, Demir (2010) [85] applied an ASR test on mortar samples prepared with the addition of silica fume and fly ash. After the experiment, it was determined that ASR occurred, elongation values increased, and compressive strength values decreased in the samples. In the samples used in this study, the development of ASR has led to cracks in the internal structure of the concrete, resulting in pressure losses.

The decrease in compressive strength values of mortar samples prepared with ASR affected by the formation of a gel with a high water retention capacity. This gel caused expansion and increased internal stresses, resulting in a loss of strength reflected in the sample results. Over time, the gel, which increased in volume by absorbing water, led to the formation of micro-cracks between the aggregate and cement paste. The continuous water absorption by the gel within the micro-crack structure further expanded the gel, enhancing and multiplying additional expansions and crack formations. Such structures in concrete or mortar have led to damage in concrete, causing reductions in mechanical properties such as compressive strength, flexural strength, and ultrasonic pulse velocity values [86–88].

5. Conclusions and Recommendations

In this study, experiments were conducted using eight different chemical composition chert aggregates from Gumushane province and one nonreactive reference aggregate (limestone). The following results have been revealed:

- The suitability of the reference sample composed of nonreactive limestone and the eight chert samples from different regions of Gumushane province for use as aggregates in concrete was evaluated in terms of ASR development. All the cherts used in the study contained high levels of reactive silica, and ASR development was not observed in all of them. In general, in the cherts that developed ASR, the fine texture of silica and the increase in the contact surface with alkali increased the ASR development.
- The chemical compositions of the cherts, which was determined using the XRF method, revealed varying amounts of reactive SiO₂ composition from high to low, resulting in the following order: AC, AK, GD, T, TD, TK, BC, GC, and R. In terms of reactive silica content, the chert called T ranks fourth, TK ranks fifth and R ranks ninth. Although reactive silica content is high in these cherts, ASR did not develop. In this case, the crystalline structure of T and TK cherts and R limestone samples is dominated by the crystalline structure of AE, while the amorphous structure is dominant in AK, GD, TK, BÇ, and SE cherts. Amorphous cherts are dominated by fractures and irregular structures, allowing ASR products to penetrate the aggregate through these irregular structures. As a result, these cherts caused the development and progression of ASR.
- Alkali equivalent amounts were calculated for the reference and eight chert samples according to ASTM C 150 standard, with values below the specified limit of 0.6%. Although the alkali content in the chert samples was below the limit value specified

in the standards, no reaction developed in the cherts expressed as TD and T, but it developed in AK, TK, GD, AÇ, BÇ, and GÇ cherts. The reason for this is the diffusion of alkali ions in the reacted cherts, gel formation in the reaction zones, and the presence of irregular internal structures that cause swelling and increase the internal stress by water absorption of the gel formed.

- The physical properties of the cherts were determined through specific surface area and sieve analysis. The highest specific surface area was found in the TD sample, with $4687 \text{ cm}^2/\text{g}$, while the lowest was in the BC sample with $889 \text{ cm}^2/\text{g}$. There was an 81.03% decrease between the highest and lowest specific surface area values. The ASR mechanisms were positively affected by specific surface area values, indicating that the TD chert sample with the highest specific surface area did not develop ASR, while the BC chert sample with the lowest specific surface area did. By comparing the ASR developments according to the specific surface area values, different situations were observed in the samples. In the TD chert sample, which has a high specific surface area, its high fineness caused less expansion, expansion rate, and amount, and ASR did not develop. The reason is that the high specific surface area value in the aggregate caused the formation of a pozzolanic reaction in the early period, converting the alkali silica gel into the calcium–silicate–hydrate formula, reducing the alkali level in the solution and causing the Pozzolanic deterioration. It was predicted that the development of alkali silica ratios in the T chert sample, which has a low specific surface area, has not yet occurred and may develop over a longer period of time. In other cherts, ASR events occurred through its textural structure and internal defects, regardless of whether the specific surface area value was high or low.
- In the conducted study, elongation values were determined according to ASTM C 1260 standard for reference and eight chert samples after curing periods of 3, 7, 14, and 28 days. Regarding ASR, samples were considered harmful aggregates if the elongation values exceeded 0.1 after the 14-day curing period and exceeded 0.2 after the 28-day curing period. According to this standard, samples denoted as R, TD, and T obtained elongation values below the threshold and were thus considered harmless aggregates in terms of ASR development. On the other hand, chert samples labeled AK, TK, GD, AC, BC, and GC were determined to exceed the specified threshold elongation values, indicating their potential for ASR development.
- After the development of ASR, thin sections were prepared to observe microstructural changes in the samples, and they were examined under a petrographic microscope. According to the obtained results, samples denoted as R, TD, and T did not exhibit ASR development, as they obtained elongation values below the threshold, and no associated crack structure was observed. On the other hand, the chert samples labeled AK, TK, GD, AC, BC, and GC showed ASR development, and under the petrographic microscope, map cracks, cracks along the aggregate, ASR gel, vesicular cracks, and fine hairline crack structures were observed. It was observed that the development of ASR in the chert samples included in the study did not depend only on the reactive silica content. Reactive silica content, specific surface area values, and the effectiveness of the grain structure were observed. In addition to these features' porosity status, AK, TK, GD, AC, BÇ and GÇ are microporous and have many lattice defects. While the potential for reaction is high, in TD and T samples, the reaction does not develop. ASR has developed in chert particles with high porosity, allowing moisture to easily penetrate and alkaline ions to disperse easily.
- Ultrasonic P-wave velocity, flexural, and compressive strength tests were conducted to determine mechanical changes in the samples after ASR development. After these tests, the quality of the concrete produced with the chert used is determined. The fact that concrete has a strong and durable feature means that a quality concrete is produced. Changes that may occur in the quality of concrete are due to the ASR formed between the aggregate and cement paste in its composition. This reaction, after a series of changes in the concrete, reduced the strength of the cement paste, causing

expansion and cracks in the concrete, and a decrease in mechanical values such as bending, pressure and ultrasonic P-wave velocity.

- Based on the ultrasonic P-wave velocity test results, it was estimated which type of concrete would be produced according to the classification expressed in studies determining concrete quality. Aggregates produced from cherts represented by T, TD, R, and AK were found to be of good quality, while concrete produced from cherts represented by GD, AC, GC, BC, BK, and TK showed moderate quality. It has been observed that ASR has not developed or has not started yet in the concretes produced with the T, TD, and AK chert samples and R (limestone) used. It has been observed that ASR started and continued in concretes produced with chert samples using GD, AC, GC, BC, BK, and TK, thus reducing the quality of the concrete.
- A flexural strength test was conducted to determine the mechanical losses of the cherts assumed to be used as aggregates in concrete after ASR. Cherts symbolized by R, TD, and T, which did not induce ASR elongation according to standards, showed the highest flexural strength values. The remaining cherts symbolized by AK, GD, AC, GC, BC, and TK showed an increase in flexural strength values as the elongation values decreased. The highest and lowest flexural strength values showed a decrease of 30.28%. Compared to the compressive strength values, the flexural strength values of the chert specimens that did not develop ASR, and the chert specimens that developed ASR did not show sharp decreases. This is because the reductions in the tensile and flexural strengths of concrete do not always occur at the same rate or rate. In these cases, it is difficult to expect a single critical expansion limit to be applicable to all structures. When considering the use of these limits, it is necessary to take into account changes in the engineering parameters of the structures, the type of aggregate, and the rate of reactivity leading to a decrease in these parameters.
- Another factor determining the mechanical strength losses of chert samples is compressive strength, which was applied to the samples. Compressive strength values, from highest to lowest, were arranged as follows: in samples in which ASR did not occur, TD, R, and T and in samples in which ASR occurred, AK, GD, AC, GC, BC, and TK. The chert sample with the highest compressive strength value belonged to the TD sample, with a value of 9.71 MPa, while the lowest compressive strength value was calculated for the TK sample at 2.76 MPa. A pressure loss of 71.6% was determined between these two samples. The use of ASR-forming cherts in concrete caused swelling and volume increase. The resulting volume increase caused tensile stresses and cracks. After the test results obtained, the lowest compressive strength value was observed in the chert sample expressed as TK. At the end of the 14- and 28-day curing periods, expansion values of 0.5% and more were obtained due to ASR formation. When chert samples with low compressive strength, such as AK, GD, AC, GC, and BC, which form ASR in concrete, were used, cracks were formed and these formations were observed in microscope images. This is because it was observed that cherts such as AK, GD, EEA, SE, and BC had expansion values higher than expansion unit deformation values such as 0.04–0.05%, which caused cracking.
- Of the eight different chert samples used in the study, five develop ASR, while three do not. It is necessary to determine which methods provide alkali silica reclamation of five different samples or which policies should be used together in the future and the method of using them as a source for regional concrete production. If this is achieved, the region will be able to produce easy-to-obtain and cost-effective concrete and meet the need for new aggregate resources in the region. To prevent ASR development of these cherts when used in new studies, the following recommendations can determine their safe use in different studies. These suggestions are as follows:
 1. Use cement with a cement alkaline component that will provide ASR formation lower than the value specified in ASTM C 150 as 0.6% Na₂O_{eq}. Deprive alkali that would enable ASR to form may prevent the reaction from occurring;

2. The use of cement with low alkalinity additives instead of the cement specified in the ASTM 1260 C standard may limit the formation of ASR reactions;
3. The cement to be added to ASR should be made of silicon-rich F class fly ashes and slag together or used separately;
4. Investigate the use of only blended cement and its effectiveness.

Funding: This research received no external funding.

Data Availability Statement: The original contributions presented in the study are included in the article.

Acknowledgments: I would like to thank the İbrahim AKPINAR of Gumushane University.

Conflicts of Interest: The author declares no conflicts of interest.

References

1. Naik, T.R. Sustainability of concrete construction. *Pract. Period. Struct. Des. Constr.* **2008**, *13*, 98–103. [[CrossRef](#)]
2. Kolawole, J.T.; Babafemi, A.J.; Paul, S.C.; du Plessis, A. Performance of concrete containing Nigerian electric arc furnace steel slag aggregate towards sustainable production. *Sustain. Mater. Technol.* **2020**, *25*, e00174. [[CrossRef](#)]
3. Adiguzel, D.; Bascetin, A.; Baray, Ş.A. Determination of Optimal Aggregate Blending to Prevent Alkali-Silica Reaction Using the Mixture Design Method. *J. Test. Eval. ASTM Int.* **2019**, *47*, 43–56. [[CrossRef](#)]
4. Figueira, R.B.; Sousa, R.; Coelho, L.; Azenha, M.; de Almeida, J.M.; Jorge, P.A.S.; Silva, C.J.R. Alkali-silica reaction in concrete: Mechanisms, mitigation and test Methods. *Constr. Build. Mater.* **2019**, *222*, 903–931. [[CrossRef](#)]
5. Davraz, M.; Gündüz, L. Reduction of alkali silica reaction risk in concrete by natural (micronised) amorphous silica. *Constr. Build. Mater.* **2008**, *22*, 1093–1099. [[CrossRef](#)]
6. Forster, S.W.; Boone, R.L.; Hammer, M.S.; Lamond, J.F.; Lane, D.S.; Miller, R.E.; Parker, S.E.; Pergalsky, A.; Pierce, J.S.; Robert, M.Q.; et al. *State-of-the-Art Report on Alkali-Aggregate Reactivity Reported by ACI Committee*; ACI Committee: Indianapolis, IN, USA, 1998; ACI 221.1R-98; pp. 1–31.
7. Latifee, E.R. State-of-the-art report on alkali silica reactivity mitigation effectiveness using different types of fly ashes. *J. Mater.* **2016**, *2016*, 7871206. [[CrossRef](#)]
8. Thomas, M.D.A.; Fournier, B.; Folliard, K.J. *Selecting Measures to Prevent Deleterious Alkali-Silica Reaction in Concrete: Rationale for the AASHTO PP65 Prescriptive Approach*; Federal Highway Administration: Washington, DC, USA, 2012.
9. *ASTM C295; Standard Guide for Petrographic Examination of Aggregates for Concrete*. ASTM International: West Conshohocken, PA, USA, 2003.
10. *ASTM C1260; Standard Test Method Potential Alkali React. Aggregates (Mortar-Bar Method)*. ASTM International: West Conshohocken, PA, USA, 2007.
11. *ASTM C 1293-08b; Standard Test Method for Concrete Aggregates by Determination of Length Change of Concrete Due to Alkali-Silica Reaction*. ASTM: West Conshohocken, PA, USA, 1995; p. 7.
12. Ichikawa, T. Alkali-silica reaction, pessimum effects and pozzolanic effect. *Cem. Concr. Res.* **2009**, *39*, 716–726. [[CrossRef](#)]
13. Diamond, S. A review of alkali-silica reaction and expansion mechanisms 1. Alkalies in cements and in concrete pore solutions. *Cem. Concr. Res.* **1975**, *5*, 329–345. [[CrossRef](#)]
14. Böhni, H. *Corrosion in Reinforced Concrete Structures*; Elsevier: Amsterdam, The Netherlands, 2005.
15. Diamond, S. A review of alkali-silica reaction and expansion mechanisms 2. Reactive aggregates. *Cem. Concr. Res.* **1976**, *6*, 549–560. [[CrossRef](#)]
16. Dent-Glasser, L.S. Osmotic Pressure and Swelling of Gels. *Cem. Concr. Res.* **1979**, *9*, 515–517. [[CrossRef](#)]
17. Dent-Glasser, L.S.; Kataoka, N. The Chemistry of AlkaliAggregate Reactions. In *Proceedings of the Fifth International Conference on Alkali-Aggregate Reactions*, Cape Town, South Africa, 30 March–3 April 1981; pp. 1–7.
18. Glasser, F.P. Chemistry of the Alkali-Aggregate Reaction. In *The Alkali-Silica Reaction in Concrete*; Swamy, R.N., Ed.; Van Nostrand Reinhold: New York, NY, USA, 1992; pp. 30–53. 333p.
19. Ichikawa, T.; Miura, M. Modified model of alkali-silica reaction. *Cem. Concr. Res.* **2007**, *37*, 1291–1297. [[CrossRef](#)]
20. Godart, B.; de Rooij, M.R.; Wood, J.G. *Guide to Diagnosis and Appraisal of AAR Damage to Concrete in Structures*; Springer: Berlin/Heidelberg, Germany, 2013.
21. Owsiak, Z. *Reakcje Kruszyw Krzemionkowych. Alkaliami w Betonie, Polski Biuletyn Ceramiczny Nr. 72*; Wydawnictwo Naukowe Akapit: Kraków, Poland, 2002. (In Polish)
22. Kurdowski, W. *Cement and Concrete Chemistry*; Springer: Dordrecht, The Netherlands, 2014.
23. Poyet, S.; Sellier, A.; Capra, B.; Foray, G.; Torrenti, J.M.; Cognon, H.; Bourdarot, E. Chemical modelling of alkali silica reaction: Influence of the reactive aggregate size distribution. *Mater. Struct.* **2007**, *40*, 229. [[CrossRef](#)]
24. Diamond, S. *Alkali Aggregate Reactions in Concrete, an Annotated Bibliography 1939–1991*; National Academy of Sciences: Washington, DC, USA, 1992.

25. Swamy, R.N. Testing for Alkali Silica Reaction. In *The Alkali-Silica Reaction in Concrete*; Swamy, R.N., Ed.; Van Nostrand Reinhold: New York, NY, USA, 1992; pp. 54–95; 333p.
26. Moundoungou, I.; Bulteel, D.; Garcia-Diaz, E.; Thiéry, V.; Dégrugilliers, P.; Hammerschlag, J.G. Reduction of ASR expansion in concretes based on reactive chert aggregates: Effect of alkali neutralisation capacity. *Constr. Build. Mater.* **2014**, *54*, 147–162. [[CrossRef](#)]
27. Islam, M.S.; Akhtar, S. A critical assessment to the performance of alkali–silica reaction (ASR) in concrete. *Can. Chem. Trans.* **2013**, *1*, 253–266.
28. Broekmans, M.A.T.M. Structural properties of quartz and their potential role for ASR. *Mater. Charact.* **2004**, *53*, 129–140. [[CrossRef](#)]
29. Lindgård, J.; Andiç-Çakır, Ö.; Fernandes, I.; Rønning, T.F.; Thomas, M.D.A. Alkali-silica reactions (ASR): Literature review on parameters influencing laboratory performance testing. *Cem. Concr. Res.* **2012**, *42*, 223–243. [[CrossRef](#)]
30. Grattan-Bellew, P.E. Petrographic and Technological Methods for Evaluation of Concrete Aggregates. In *Handbook of Analytical Techniques in Concrete Science and Technology Principles, Techniques and Applications*; Ramachandran, V.S., Beaudoin, J.J., Eds.; Noyes Publication: Park Ridge, NJ, USA, 2001; pp. 63–98.
31. Bérubé, M.-A.; Fournier, B. Canadian experience with testing for alkaliaggregate reactivity in concrete. *Cem. Concr. Compos.* **1993**, *15*, 27–47. [[CrossRef](#)]
32. Farny, J.A.; Kosmatka, S.H. *Diagnosis and Control of Alkali-Aggregate Reactions in Concrete*; Concrete Information; Portland Cement Association: Washington, DC, USA, 1997; 23p.
33. ACI. *State of the Art Report on Alkali Aggregate Reactivity*; ACI Committee 221; ACI: Indianapolis, IN, USA, 1998; 31p.
34. Thomas, M.D.A.; Fournier, B.; Folliard, K.J.; Ideker, J.H.; Resendez, Y. *The Use of Lithium to Prevent or Mitigate Alkali-Silica Reaction in Concrete Pavements and Structures*; Turner-Fairbank Highway Research Center: McLean, VA, USA, 2007.
35. Multon, S.; Cyr, M.; Sellier, A.; Diederich, P.; Petit, L. Effects of Aggregate Size and Alkali Content on ASR Expansion. *Cem. Concr. Res.* **2010**, *40*, 508–516. [[CrossRef](#)]
36. Stanton, T.E. *Expansion of Concrete through Reaction between Cement and Aggregate*; American Concrete Institute (ACI): Country Club Drive Farmington Hills, MI, USA, 2008; Available online: <http://worldcat.org/isbn/9780870312694> (accessed on 7 February 2024).
37. Ben Haha, M.; Gallucci, E.; Guidoum, A.; Scrivener, K.L. Relation of expansion due to alkali silica reaction to the degree of reaction measured by SEM image analysis. *Cem. Concr. Res.* **2007**, *37*, 1206–1214. [[CrossRef](#)]
38. Kuroda, T.; Inoue, S.; Yoshino, A.; Nishibayashi, S. Effects of particle size grading and content of reactive aggregate on ASR expansion of mortars subjected to autoclave method. In Proceedings of the 12th International Conference on Alkali-Aggregate Reaction in Concrete, Beijing, China, 15–19 October 2004.
39. Wigum, B.J.; Lindgård, J. AAR: Testing, mitigation & recommendations. The Norwegian approach during two decades of research. In Proceedings of the 13th International Conference on Alkali-Aggregate Reaction in Concrete, Trondheim, Norway, 16–20 June 2008; pp. 1299–1309.
40. Saha, A.K.; Khan, M.N.N.; Sarker, P.K.; Shaikh, F.A.; Pramanik, A. The ASR mechanism of reactive aggregates in concrete and its mitigation by fly ash: A critical review. *Constr. Build. Mater.* **2018**, *171*, 743–758. [[CrossRef](#)]
41. Mehta, P.K.; Monteiro, P.J.M. *Concrete Microstructure, Properties and Materials*; Prentice-Hall Inc.: Englewood Cliffs, NJ, USA, 1993; 659p.
42. Helmuth, R.; Stark, D. Alkali-Silica Reactivity Mechanisms. In *Materials Science of Concrete III*; Skalny, F., Ed.; The American Ceramic Society: Westerville, OH, USA, 1992; pp. 131–138.
43. Zhang, C.; Wang, A.; Tang, M.; Wu, B.; Zhang, N. Influence of Aggregate Size and Aggregate Size Grading on ASR Expansion. *Cem. Concr. Res.* **1999**, *29*, 1393–1396. [[CrossRef](#)]
44. Ramyar, K.; Topal, A.; Andiç, Ö. Effects of Aggregate Size and Angularity on Alkali-Silica Reaction. *Cem. Concr. Res.* **2005**, *35*, 2165–2169. [[CrossRef](#)]
45. Andiç-Çakır, Ö. Investigation of Test Methods on Alkali Aggregate Reaction. Ph.D. Thesis, Ege University, Department of Civil Engineering, Bornova, Türkiye, 2007; 252p.
46. Chatterji, S. Chemistry of alkali-silica reaction and testing of aggregates. *Cem. Concr. Compos.* **2015**, *27*, 788–795. [[CrossRef](#)]
47. Islam, M.S.; Ghafoori, N. Relation of ASR-induced expansion and compressive strength of concrete. *Mater. Struct.* **2015**, *48*, 4055–4066. [[CrossRef](#)]
48. McNally, C.; Richardson, M.G. Reactivity assessment of aggregates: Role of chert crystallinity. *ACI Mater. J.* **2005**, *102*, 163–169.
49. Rajabipour, F.; Giannini, E.; Dunant, C.; Ideker, J.H.; Thomas, M.D.A. Alkali–silica reaction: Current understanding of the reaction mechanisms and the knowledge gaps. *Cem. Concr. Res.* **2015**, *76*, 130–146. [[CrossRef](#)]
50. Aşık, İ.; Şen, H.; Ergintav, Y.; Ünsal, A.; Şentürk, E.; Bayrak, E. *Rehabilitation of the Agregate Harmful in Respect of Alkali Silica Reation*; Concrete Congress: Ankara, Turkey, 2004.
51. Alexander, M.G.; Mindness, S. *Aggregates in Concrete (Modern Concrete Technology)*; CRC Press: Boca Raton, FL, USA, 2005; 448p.
52. Thomas, M.D.A.; Fournier, B.; Folliard, K.J.; Resendez, Y. *Alkali-Silica Reactivity Field Identification Handbook*; Federal Highway Administration, Office of Pavement Technology: Washington, DC, USA, 2011.
53. Lima, M.; Salamy, R.; Miller, D. CFRP strengthening of ASR affected concrete piers of railway bridges. In *Maintenance, Safety, Risk, Manag. Life-Cycle Performance of Bridges, Proceedings of the Ninth International Conference on Bridge Maintenance, Melbourne, Australia, 9–13 July 2018*; CRC Press: Boca Raton, FL, USA, 2018; p. 346.

54. Fanijo, E.O.; Kolawole, J.T.; Almakrab, A. Alkali-silica reaction (ASR) in concrete structures: Mechanisms, effects and evaluation test methods adopted in the United States. *Case Stud. Constr. Mater.* **2021**, *15*, e00563. [CrossRef]
55. Deschenes, D.J.; Bayrak, O.; Folliard, K.J. *ASR/DEF-Damaged Bent Caps: Shear Tests and Field Implications*; Technical Report No. 12-18XXIA006; University of Texas: Austin, TX, USA, 2009; 258p.
56. Snyder, K.A.; Lew, H.S. *Alkali-Silica Reaction Degradation of Nuclear Power Plant Concrete Structures: A Scoping Study*; National Institute of Standards and Technology Engineering Laboratory: Gaithersburg, MD, USA, 2013.
57. Bektasa, F.; Turanlia, L.; Topal, T.; Goncuoglu, M.C. Alkali reactivity of mortars containing chert and incorporating moderate-calcium fly ash. *Cem. Concr. Res.* **2004**, *34*, 2209–2214. [CrossRef]
58. Williams, H.; Turner, F.J.; Gilbert, C.H. *Petrography*; Freeman: New York, NY, USA, 1982.
59. Wigum, B.J. Alkali-Aggregate Reactions in Concrete: Properties, Testing and Classification of Norwegian Cataclastic Rocks. Ph.D. Thesis, University of Trondheim, Trondheim, Norway, 1995.
60. Richardson, M. Minimising the risk of deleterious alkali-silica reaction in Irish concrete practice. *Constr. Build Mater.* **2005**, *19*, 654–660. [CrossRef]
61. Nishiyama, T.; Kusuda, H.; Nakano, K.A. Few remarks on alkalireactive chert aggregates. In Proceedings of the Eighth International Conference on Alkali-Aggregate Reaction, Kyoto, Japan, 17–20 July 1989; Okada, K., Nishibayashi, S., Kawamura, M., Eds.; pp. 543–548.
62. Jones, T.N. Mechanism of reactions involving British chert and flint aggregates. In Proceedings of the Eighth International Conference on Alkali-Aggregate Reaction, Kyoto, Japan, 17–20 July 1989; Okada, K., Nishibayashi, S., Kawamura, M., Eds.; pp. 135–140.
63. Larbi, J.A.; Visser, J.H.M. A study of the ASR of an aggregate with high chert content by means of ultra accelerated mortar bar test and pore fluid analysis. *Heron* **2002**, *47*, 141–159.
64. Gogte, B.S. An evaluation of some common Indian rocks with special reference to alkali aggregate reactions. *Eng. Geol.* **1973**, *7*, 135–154. [CrossRef]
65. Fournier, B.; Chevier, R.; De Grosbois, M.; Lisella, R.; Folliard, K.; Idekar, J.; Shehata, M.; Thomas, M.; Baxer, S. The Accelerated Concrete Prism Test (60 °C): Variability of the Test Method and Proposed Expansion Limits. In Proceedings of the 12th International Conference on Alkali-Aggregate Reaction in Concrete, Beijing, China, 15–19 October 2004; Tang, M., Deng, M., Eds.; World Publishing Corporation: Beijing, China, 2004; pp. 314–323.
66. *ASTM C 597*; Designation: C597-09 Standard Standard Test Method for Pulse Velocity Through Concrete. ASTM International: West Conshohocken, PA, USA, 2010.
67. *TS EN 196-1*; Çimento Deney Yöntemleri, Dayanım Tayini. Türk Standartları Enstitüsü: Ankara, Turkey, 2002.
68. *TS EN 196-2*; Çimento Deney Yöntemleri—Bölüm 2: Çimentonun Kimyasal Analizi. Türk Standartları Enstitüsü: Ankara, Turkey, 2013.
69. *ASTM C 150*; Standard Specification for Portland Cement. ASTM: West Conshohocken, PA, USA, 2005; p. 8.
70. Wang, H.; Gillott, J.E. Effect of some chemicals on alkali silicareaction. In Proceedings of the 9th International Conference on Alkali-Aggregate Reaction, London, UK, 27–31 July 1992; Concrete Society of UK: London, UK, 1992; pp. 1090–1099.
71. Yalçın, H.; Özalp, R. *Alkali-Agrega Reaction in Concrete and Alkalinity Values of Turkish Cements*; State Hydraulic Works Publication: Ankara, Turkey, 1974.
72. Mindess, S.; Young, J.F. *Concrete*; Prentice-Hall, Inc.: Hoboken, NJ, USA, 1981.
73. Xu, H. On the alkali content of cement in AAR, Concr. Alkali-Aggregate React. In *Proceedings of the 7th International Conference*; Grattan-Bellew, P.E., Ed.; Noyes Publications: Park Ridge, NJ, USA, 1987; pp. 451–455.
74. Bérubé, M.-A.; Frenette, J. Testing concrete for AAR in NaOH and NaCl solutions at 38 C and 80 C. *Cem. Concr. Compos.* **1994**, *16*, 189–198. [CrossRef]
75. Ramyar, K.; Dönmez, H.; Andiç, Ö. *Control of Alkali Silica Reaction by Mineral and Chemical Additives*; Turkish Cement Manufacturers' Association, Cement and Concrete Research and Development Institute: Ankara, Turkey, 2002.
76. Da Thomas, M.; Fournier, B.; Folliard, K.J. *Alkali-Aggregate Reactivity (AAR) Facts Book*; Federal Highway Administration, Office of Pavement Technology: Washington, DC, USA, 2013.
77. Woods, H. *Durability of Concrete Construction, Monograph No. 4*; American Concrete Institute: Detroit, MI, USA, 1968.
78. SHRP. Alkali Silica Reactivity Library Handbook for Identification ASR. U.S. Department of Transportation Federal Aviation Administration, 2004. Available online: <https://leadstates.tamu.edu/asr> (accessed on 7 February 2024).
79. Nishibayashi, S.; Yamura, K. Effect of reactive fine aggregate on expansion characteristics of concrete due to alkali aggregate reaction. In Proceedings of the 9th International Conference on Alkali-Aggregate Reaction in Concrete, London, UK, 27–31 July 1992; pp. 723–730.
80. Sims, I.; Nixon, P. RILEM recommended test method AAR-1: Detection of potential alkali reactivity of Aggregates-Petrographic method. *Mater. Struct.* **2003**, *36*, 480–496. [CrossRef]
81. Binal, A. The investigation of effects of pessimum reactive aggregate content on alkali-silica reaction with experimental methods. *Istanb. Univ.-Turk. Eng. Fak. J. Earth Sci.* **2004**, *17*, 119–128.
82. Eker, H.; Demir Şahin, D.; Çullu, M. Effect of Reduced Fineness of Fly Ash Used on the Alkali-Silica Reaction (ASR) of Concrete, Iranian Journal of Science and Technology. *Trans. Civ. Eng.* **2023**, *47*, 2203–2217. [CrossRef]
83. Whitehurst, E.A. Soniscope Test Concrete Structures. *J. Am. Concr. Inst. Proc.* **1951**, *47*, 443–444.

84. Uyanık, O.; Kaptan, K.; Gülay, F.G.; Tezcan, S. Determination of Concrete Strength by Non-Destructive Ultrasonic Method. *World Constr.* **2011**, *184*, 55–58.
85. Demir, İ. The mechanical properties of alkali-silica reactive mortars containing same amounts of silica fume and fly ash. *Gazi Univ. J. Fac. Eng. Archit.* **2010**, *25*, 749–758.
86. Swamy, R.N.; Al-Asali, M.M. Expansion of concrete due to ASR. *ACI Mater. J.* **1988**, *85*, 33–40.
87. Neville, A.M. *Properties of Concrete*; Longman Scientific & Technical: Harlow, UK, 1981.
88. Gümüş, S. Determining the Alkali—Agrega Reactivity of the Aggregates at Kocaeli Region. Master's Thesis, Sakarya University Institute of Science and Technology, Sakarya, Türkiye, 2009.

Disclaimer/Publisher's Note: The statements, opinions and data contained in all publications are solely those of the individual author(s) and contributor(s) and not of MDPI and/or the editor(s). MDPI and/or the editor(s) disclaim responsibility for any injury to people or property resulting from any ideas, methods, instructions or products referred to in the content.